Through symmetry breaking to higher dimensional chaotic scattering

Inauguraldissertation

zur

Erlangung der Würde eines Doktors der Philosophie

vorgelegt der

Philosophisch-Naturwissenschaftlichen Fakultät
der Universität Basel

von

Olivier Merlo
aus Aarberg BE

Hölstein, 2004

Genehmigt von der Philosophisch-Naturwissenschaftlichen Fakultät
auf Antrag der
Herren Professoren Dr. Dirk Trautmann und Dr. Thomas H. Seligman

Basel, den 6. Dezember 2004

Prof. Dr. Marcel Tanner

Dekan

Abstract

The goal of this thesis is to gain some insight into chaotic scattering dynamics in systems with more than two effective degrees of freedom. We use the idea of "gradually" introducing another degree of freedom by perturbating slightly a symmetry that has reduced a three–dimensional system to two effective dimensions.

We furthermore specifically study the case of a system where a particle was scattered by a hard disc moving on a circle which will be slightly deformed to an ellipse. This leads to a slight violation of the Jacobi integral which causes the increase of dimension of phase space.

We first complement previous studies of the problem with symmetry by showing elliptic areas, obtaining linear response results and the bifurcation scenario.
Then we show how analyzing spaces of initial conditions in terms of the number of the scattering events before ejection yields information about periodic orbits, stable or longlived islands and bifurcations. This allows us to gain considerable insight into the scattering process, that can be of use in qualitative understanding of planetary rings in celestial mechanics and seems to be valid far beyond the toy model we use.

Zusammenfassung

Das Ziel dieser Dissertation ist einen Einblick in chaotische Streusysteme mit mehr als 2 effektiven Freiheitsgraden zu bekommen. Wir benutzen die Idee, dass durch eine kleine Perturbation einer Symmetrie ein zusätzlicher Freiheitsgrad eingeführt wird. Der symmetrische Fall des untersuchten Systems besitzt zwei Freiheitsgrade, welche durch Brechung der Symmetrie auf drei ansteigt.

Wir studieren den Fall der Streuung eines Teilchens an einer harten Scheibe, welche sich auf einer kreisförmigen Bahn bewegt. Die Symmetriebrechung kommt durch eine Deformation der kreisförmigen Bahn zustande. Diese Symmetriebrechung bewirkt, dass das Jacobi–Integral keine Erhaltungsgrösse mehr ist und damit die Anzahl der Freiheitsgrade um eins erhöht wird.

Zuerst vervollständigen wir vorherige Studien des symmetrischen Streuproblems. Wir zeigen die Existenz von elliptischen Regionen im Phasenraum. Zusätzlich werden Resultate der linearen Approximation und das Bifurkationsszenario gegeben. Danach zeigen wir, wie man Informationen über periodische Bahnen, stabile oder langlebige Inseln und Bifurkationen aus zwei dimensionalen Streukarten erhält. Dies erlaubt es uns beträchtliche Einblicke in den Streuprozess zu erhalten, welche zum besseren Verständniss von planetaren Ringen führt. Die Resultate scheinen viel allgemeiner zu sein, als nur für das untersuchte toy Modell.

Contents

Chapter 1

Preface

The classical dynamics of scattering systems, in particular its chaotic manifestations, is well understood for open Hamiltonian systems with two effective degrees of freedom. Typical examples are one–dimensional periodically–kicked driven systems and conservative (time–independent) systems of two degrees of freedom. The effective dimension of phase space is then three. In such cases, the dynamics is determined by the properties of the invariant set or chaotic saddle. Smale's horseshoe construction can then be performed on an appropriate surface of section [1, 2], and explains adequately the topology and symbolic dynamics of such a problem.

Unfortunately, the situation becomes qualitatively more complex for higher dimensions. It is not only that the surface of section is no longer two dimensional, and thus not easy to draw and understand, but also fundamental differences occur. For example invariant tori (KAM-surfaces [3]) no longer separate the phase space, giving rise to Arnold diffusion [4], and in addition to hyperbolic and elliptic fixed points also loxodromic fixed points can appear. Wiggins and co–workers [5] have made some progress in characterizing the invariant manifolds of Hamiltonian flows in higher dimensions.
They studied the special case of systems with one outer fixed point. This fixed point has 2 characteristic multipliers of absolute value different from one and the remaining characteristic multipliers are of absolute value of one. In these cases the edges of the fundamental rectangle are given by the normally hyperbolic invariant manifolds. These normally hyperbolic invariant manifolds are constructed using the unstable resp. stable manifold and the center manifold. If the outer fixed point does not belong to the above classe of fixed point, no suggestions how to define the fundamental hyper–cube are known.

Yet we are far from a useful understanding of the chaotic saddle in higher–dimensions.

In a scattering system with two effective degrees of freedom scattering functions are a important tool to get informations of the scattering system [6, 7, 8, 9].

In a high–dimensional space of initial conditions, the choice of the subspace to get useful scattering functions requires a considerable physical insight, or plain luck, to an unreasonable degree. We shall thus concentrate on a particular, but very important situation, where the physical insight is systematically available.

Dimensional reduction of a system is possible if a continuous symmetry is given, leading to a conserved quantity. We can therefore hope that a slight breaking of such a symmetry, while putting us abruptly in a higher–dimensional space, will nevertheless leave an important mark on the system, that will in some sense slowly vanish as symmetry breaking increases. On the other hand, this case is certainly not irrelevant, but rather occurs quite frequently in practice.

We consider here the example of the restricted three–body problem. The constant of motion in question is the Jacobi integral [10] which is conserved, when the orbits of the two heavy bodies are exactly circular. While this is probably never the case in a real system, small eccentricities of orbits are quite common.

Chapter 2

Introduction

2.1 General overview

In Chapter 1 and 2 we will use the following notations:

Symbol	explanation
n	Number of degrees of freedom
P	Phase space
q_i and p_i	coordinates
I and θ	action-angle coordinates
H	Hamiltonian $H : P \to \mathbb{R} \in \mathcal{L}^2$
$\mathbf{x}$	general point in phase space
b	impact parameter
t	time

H will be the generating function of the dynamics. The time–evolution is given by

$$\frac{dq_i}{dt}(t) = \frac{\partial H}{\partial p_i} \text{ and } \frac{dp_i}{dt}(t) = -\frac{\partial H}{\partial q_i}. \tag{2.1}$$

The point $\mathbf{x}(t) = (q_1(t), \ldots, q_n(t), p_1(t), \ldots, p_n(t))^T$ is defined if the vector field is not singular and will not go to infinity in finite times. The equation (2.1) can then be rewritten as

$$\frac{d\mathbf{x}(t)}{dt} = \mathbf{J}\, DH(\mathbf{x}), \tag{2.2}$$

where DH is the derivative of H with respect to $\mathbf{x}$ and $\mathbf{J}$ is given by

$$\mathbf{J} = \begin{pmatrix} 0 & \mathbf{I}_n \\ -\mathbf{I}_n & 0 \end{pmatrix} \tag{2.3}$$

with the $n \times n$ identity matrix $\mathbf{I}_n$.
The time t defines a one–parameter group (flow map) $\phi_t : P \to P$ on P.

2.2 Conserved quantities

A quantity K is conserved if the function $K : P \to \mathbb{R}$ satisfies the condition

$$0 = \frac{d}{dt}K = \{K, H\}, \text{ with } \{F, G\} = \sum_{i=1}^{n} \left(\frac{\partial F}{\partial q_i}\frac{\partial G}{\partial p_i} - \frac{\partial G}{\partial q_i}\frac{\partial F}{\partial p_i} \right). \tag{2.4}$$

If the Hamiltonian is not time–dependent then the energy H is a conserved quantity.

2.3 Complete integrability of a system

A system with n degrees of freedom is called completely integrable [11], if n conserved quantities $(K_1, \ldots, K_n)$ exists with $K_i \in C^\infty(K_i : P \to \mathbb{R})$ which only depend on a set of measure 0, i.e.,

$$\int \{K_i, K_j\} d\mu(A) = 0, \forall i, j, i \neq j. \tag{2.5}$$

The Liouville-Arnold theorem states that the dynamics of a completely integrable system on a compact connected manifold is then given in action angle variables $(I, \theta) \in \mathbb{R}^n \times T^n$ by

$$\begin{aligned} \dot{I} &= -D_\theta H = 0 \\ \dot{\theta} &= D_I H, \end{aligned} \tag{2.6}$$

where T^n is the n-dimensional torus, D_θ resp. D_I is the derivative of the Hamiltonian with respect to θ resp. I.

2.4 Poincaré map

Consider the system (2.2) with a periodic orbit γ with period τ and a point $\mathbf{y} \in \gamma$ of the periodic orbit. Now define a surface Σ transverse to the vector field in the vicinity of $\mathbf{y}$. Transverse means that the vector field is never parallel to the surface Σ. The Poincaré map is defined as the map which associates points on Σ with points on Σ due to the flow ϕ_t generated by the Hamiltonian (2.2).
The Poincaré map allows to study a $n' - 1$ dimensional map instead of a n' dimensional flow.

2.5 Characteristic multipliers of symplectic maps

If a Hamiltonian systems is reduced by the method of the Poincaré map a symplectic map [11] is obtained, where the matrix $\mathbf{S}$ of the derivative has the property

$$\mathbf{S}^T \mathbf{J} \mathbf{S} = \mathbf{J}. \tag{2.7}$$

There are only three possibilities for the characteristic multipliers of fixed points of symplectic maps. This can easily be seen using the property

$$\det(\mathbf{S} - \lambda \mathbf{I}_{2n}) = \lambda^{2n} \det(\mathbf{S} - \frac{1}{\lambda} \mathbf{I}_{2n}). \tag{2.8}$$

This equation (2.8) shows that if λ is an eigenvalue, then $1/\lambda$ is an eigenvalue, too. Here λ can either be real or complex. If λ is complex and lies on the unit circle, so $1/\lambda = \overline{\lambda}$ lies on the unit circle as well. If λ does not lie on the unit circle then eigenvalues $\overline{\lambda}$, $1/\overline{\lambda}$ and $1/\lambda$ must exist, since the matrix elements are real. This latter case is called the loxodromic case.

2.6 Bifurcations of symplectic maps

From the characteristic multipliers (see section 2.5) of symplectic maps it is clear that there can be maximally three bifurcations or combinations of them. If the map has two complex eigenvalues on the unit circle, then (λ, $\overline{\lambda}$) can meet each other at 1 or -1. If they coincide, one can either gets a stable and a unstable direction of the fixed point or nothing changes. If the eigenvalues are -1 a period doubling bifurcation can occur [12, 13, 14].

For the case if the map has four characteristic multipliers, that coincide in pairs on the unit circle, Krein [12] showed that a bifurcation can only occur, if the Krein signature

$$Kr(\vec{\psi}) = < \mathbf{J}.\vec{\psi}, \vec{\psi} > \tag{2.9}$$

on the subspaces corresponding to the eigenvalues is not of definite sign. Thus the twofold eigenvalues λ and $\overline{\lambda}$ can bifurcate to eigenvalues $\lambda_1,\ \overline{\lambda}_1,\ 1/\lambda_1,\ 1/\overline{\lambda}_1$.

Chapter 3

Scattering system

A scattering system generally satisfies the two following conditions:

1. At least one degree of freedom in q-space must be open
2. $H_0 = \lim_{q\to\infty} H$, where H_0 is integrable and $\lim_{q\to\infty} q|H_0 - H| \to 0$

The second condition is satisfied by a potential which decreases faster than $1/r$.

3.1 Scattering

If E is the set of asymptotes , then the entire scattering process is a mapping from E to E, excluding a subset of measure zero [15, 16].

3.2 Scattering function

A scattering function is a function along a parameter in the asymptotic region of a measurable parameter. Of special importance is the time–delay function, which is defined as the measured time minus the asymptotic time.
Now there is the question how to choose this parameter. We will define H_0 such that we have $n-1$ integrals of motion, so we can label the $2\,n$ coordinates by the integral of motion, the corresponding angles, and the impact parameter b.

3.3 Scattering system with two degrees of freedom

If a scattering system has two degrees of freedom and the Hamiltonian is time independent, then the Poincaré map is two dimensional. The discussion is restricted

to one open channel, here. If the system has one open channel then the Poincaré map has one outer fixed point which must be hyperbolic, because the system is hamiltonian and the outer fixed points necessarily have a stable and an unstable manifold (due to the remarks in section 2.5 and the Hartman Grobman theorem [17, 18]). This invariant manifold defines the fundamental region of the scattering. Rückerl et al [19] have investigated a case with one open channel and one inner fixed point in detail.

3.4 The higher–dimensional case

The scattering systems which can be reduced due their symmetry and the method of the Poincaré map to a two dimensional map are well understood. There are three fundamental reasons why higher–dimensional maps are much more complicated. First, one can draw pictures which can be interpreted quite easily in two dimensions. For maps with more than two dimensions only projections can be drawn. Second, in order to have a scattering system at least one fixed point with a stable and an unstable direction is required. In a n–dimensional map, the barriers which define the fundamental region must be $n-1$ dimensional. Additionally, the barriers have to be an invariant set [20]. A set A is called invariant under the map $x \to f(x)$ if for any $x \in A$, $f^m(x) \in A \, \forall m \in \mathbb{Z}$ is satisfied. Third, the KAM surfaces no longer separate the phase space, allowing for Arnold diffusion [4].

In the two dimensional case the map has an unstable and a stable manifold of dimension one. These manifolds can be used to form the barriers in phase space which define the fundamental region. In higher–dimensional symplectic maps the fixed points can have the combinations of characteristic multipliers mentioned in section 2.5.

For a system having a fixed point with one pair of real characteristic multipliers and m pairs of imaginary characteristic multipliers with magnitude 1, Wiggins *et al*. [5, 21] have proposed the following barriers in phase space. They define one barrier with the invariant manifold formed by the unstable and the center manifold of the outer fixed point. Another barrier is given by the stable and the center manifold of the outer fixed point. Both manifolds are of dimension $2\,m+1$, invariant and are called normally hyperbolic invariant manifold. This kind of barriers or invariant manifolds are closely related to the stable and the unstable manifold of the two dimensional case.

In the present study, we are dealing with systems where a constant of motion vanishes due to symmetry breaking, and thus the phase space gets extended. The eigenvalues of the periodic orbits corresponding to the integral of motion are 1 in

the symmetric case.
For weak breaking of the symmetry, one might expect the phase space region where one finds characteristic scattering functions from the scattering functions of the symmetric case.

3.4.1 Further problems

The three-dimensional (3D) case already shows a lot of the problems which arise in higher dimensions. One can construct a 3D map where the determinant of the derivative is 1 with one outer fixed point with a 1D stable and a 2D unstable manifold. The map consists of first stretching and folding in one direction and afterwards stretching and folding in another direction. So the mapping looks like in Figure 3.1. A similar picture can be find in the book [22] by Wiggins on page 260. For this map, the problem is to define the fundamental region or , rather, the border of it. Apparently, Wiggins assumes that that the 1D unstable manifolds corresponding to the eigenvalues λ_1 and λ_2 meet the stable manifold at one point. This is equivalent to the statement that the edges of the fundamental region are defined by the 1D unstable manifold given by the eigenvectors λ_1, λ_2.

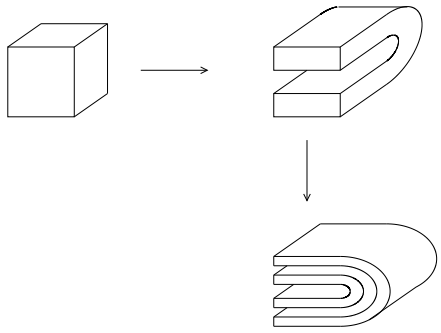

Figure 3.1: 3D horseshoe map

This is usually not the case. In contrast, usually not even one of these 1D unstable manifolds meet the stable manifold. So the edges should belong to the 2D unstable manifold and should be invariant. In a linearized map with eigenvalues λ_1 resp. λ_2 in the x resp. y direction one of the easiest invariant manifold is given by

$$\begin{pmatrix} x \\ y \end{pmatrix} = \begin{pmatrix} t \\ c\,t^{\frac{\ln(\lambda_2)}{\ln(\lambda_1)}} \end{pmatrix}, \tag{3.1}$$

where $t \in \mathbb{R}^+$ is a parameter and c a constant.
In the map we have investigated, we have seen that the edges cannot be given in this way.

3.5 The escape rate

We consider an ensemble of initial conditions N^0 far away of the interaction region and look which fraction $N(t)$ of the ensemble N^0 is still in the interaction region after the time t for asymptotic long times. It can be shown that for hyperbolic systems [23, 24] this fraction has an exponential dependence,

$$N(t) \sim \exp(-\kappa\, t). \tag{3.2}$$

Here the constant κ is called the escape rate.

If there is at least one elliptic region, then an algebraic escape law [25, 26, 27] applies,

$$N(t) \sim t^{-\alpha} \tag{3.3}$$

where the exponent α is roughly between 1.2-1.5 [28].

Chirikov and Shepelyansky [29] have shown that in the standard map with the critical rotation number $((\sqrt{5}-1)/2)$, the exponent for the Poincaré recurrence time is 3. It is believed that for higher coupling strengths all invariant KAM-curves are destroyed [29]. The Poincaré recurrence time is closely related to the escape rate.

From the equations (3.2) and (3.3) it is clear that the differential escape $\frac{\partial N(t)}{\partial t}$ follows the same law, but with another exponent for the algebraic escape rate.

Consider now an ensemble of initial conditions in the interaction region. Then for asymptotic long times the differential escape follows the same law as described above, but if there are stable islands then there is an ensemble proportional to the relative volume of the stable islands which never escapes. So if a stable island exists, then this should be seen in the tail of the differential escape rate.

Chapter 4

The toy model

Benet $et\,al.$ [30] have investigated the scattering of a point-like particle at a disc moving on a circular orbit. See Figure 4.1 for a sketch of the geometry and for the definition of different terms. The angle ϕ is given by the position of the disc on the orbit. Additionally two angles α and θ are defined which are given just after the reflection of the projectile on the disc. We define $\alpha \in [0, 2\,\pi[$ as the angle between the vector pointing to the middle of the disc and the vector from the middle of the disc pointing to the reflecting point on the disc. We further define the angle $\theta \in [0, 2\,\pi]$ as the angle between the velocity vector and the vector pointing to the middle of the moving disc. The definition domain of the angle θ is a little bit more complicated because the velocity is not taken in the moving frame. Dullin [31] has shown that it is possible to define a symplectic map in a billiard system with potentials.

We will focus our attention to discs moving on elliptic keplerian orbits with small eccentricity and the circular orbit. In section 4.1 and 4.2, we will show some general results. In section 4.3, we present the case of a disc moving on a circular orbit. We then consider the disc moving on an elliptic keplerian orbit in section 4.4.

4.1 Coordinate transformation

In Figure 4.1, the geometry of the toy model is shown. The disc with radius d is moving on an orbit around the origin of the coordinate system. The center of the disc is at a distance $R(\phi)$ from the origin. The angle which describes the position of the disc is denoted by ϕ and the angular velocity of the disc is $\dot{\phi}$. Thus, the movement of the center of the disc can be described by

$$\vec{X}_R = R(\phi)\,\vec{n}(\phi), \tag{4.1}$$

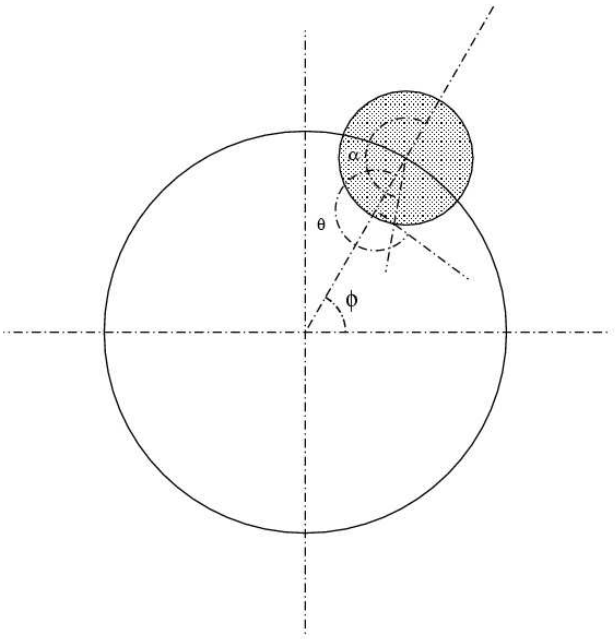

Figure 4.1: Geometry of the model.

where

$$\vec{n}(\phi) = (\cos(\phi), \sin(\phi))^T \tag{4.2}$$

is the normal vector with the angle ϕ relative to the x-axis.

The toy system is described by the Hamiltonian

$$H = \frac{P_x^2 + P_y^2}{2} + V_d(\vec{X}_R, \vec{X}), \tag{4.3}$$

where the potential V_d is infinite for $(\vec{X}_R - \vec{X})^2 \leq d^2$, X resp. Y are the spatial coordinates and P_x resp. P_y are the corresponding momenta. Because the potential depends explicitly on time through the position of the disc $\vec{X}_R$, the Hamiltonian H is not a constant of motion.

Meyer *et al.* [30] used the generating function

$$W = P_x \left(x \cos(\omega\, t) - y \sin(\omega\, t)\right) + P_y \left(y \cos(\omega\, t) + x \sin(\omega\, t)\right), \tag{4.4}$$

with the angular velocity ω to get a new Hamiltonian (4.17). This corresponds to transforming into a rotating frame (synodic frame). The generating function

$$W_g = \left(P_x \left(x \cos(\phi) - y \sin(\phi)\right) + P_y \left(y \cos(\phi) + x \sin(\phi)\right)\right) \frac{R(\phi)}{\overline{R}} \tag{4.5}$$

is a more general transformation for the Hamiltonian under the above assumptions, where $\overline{R}$ is the mean radius of the orbit of the disc.
Using the generating function (4.5) the Hamiltonian

$$J_g = \frac{\overline{R}^2}{2\,R(\phi)^2}\,\vec{p}^2 - \dot{\phi}\,(x\,p_y - y\,p_x) - <\vec{r},\vec{p}> \frac{\dot{\phi}}{R(\phi)}\frac{\partial R(\phi)}{\partial \phi} + V_d\left(\begin{pmatrix}\overline{R}\\0\end{pmatrix},\vec{r}\right) \tag{4.6}$$

is obtained, where the disc is at rest at $\left(\overline{R},\ 0\right)^T$, $\vec{r}$ is the position vector, $\vec{p}$ the conjugate momentum, and $<,>$ the usual scalar product.

4.2 Periodic orbits

In this section here, we prove the existence of the periodic orbits in the problem of scattering off a disc on an orbit, which is a perturbation of a circular orbit, adapting the method of analytical continuation [32] for this billiard problem.
Consider that the particle collides with the disc. The collision is described by means of the angles ϕ, α and θ (defined in Figure 4.1) and the Jacobi integral $\tilde{J}$ (4.17) in the rest frame. The movement of the center of the disc will be described by

$$\vec{R}(\phi) = R\,\vec{n}(\phi) + \varepsilon\,\vec{g}(\phi), \tag{4.7}$$

where the perturbation of the circular orbits is described by $\vec{g}(\phi)$.

Additionally it is assumed that the function $\vec{g}(\phi)$ is a Fourier series in ϕ. The time dependence of ϕ is given by

$$t = \phi + \varepsilon\,h(\phi), \tag{4.8}$$

where $h(\phi)$ can be decomposed in a Fourier series, too.

Given the n–th collision, the collision $n+1$, which is assumed to take place, is defined by the map f_ε,

$$\begin{pmatrix}\phi_{n+1}\\ \alpha_{n+1}\\ \theta_{n+1}\\ \tilde{J}_{n+1}\end{pmatrix} = f_\varepsilon \begin{pmatrix}\phi_n\\ \alpha_n\\ \theta_n\\ \tilde{J}_n\end{pmatrix}. \tag{4.9}$$

In the circular case, the fixed points of this map correspond to periodic orbits if the angle θ satisfies the relation (see section 4.3.2)

$$\theta = \frac{\pi}{2\,m}(2\,p + m - 2\,n\,m), \tag{4.10}$$

where p, m and n are $0, 1, 2, \ldots$. In this case, the periodic orbit is closed after m bounces with the disc, and n denotes the number of full turns of the disc between consecutive bounces. In particular, for the circular case,

$$f_0 \begin{pmatrix} \phi_n \\ \pi \\ \theta_n \\ \tilde{J}_n \end{pmatrix} = \begin{pmatrix} \phi_n + \delta\phi \bmod(2\pi) \\ \pi \\ \theta_n \\ \tilde{J}_n \end{pmatrix}, \tag{4.11}$$

where $\delta\phi = (2\,n-1)\pi + 2\,\theta$ is the difference in the angle ϕ between two successive bounces.

We are now going to prove the existence of initial conditions that are mapped onto themselves after m bounces. This condition is fulfilled if

$$f_\varepsilon^m \begin{pmatrix} \phi \\ \alpha \\ \theta \\ \tilde{J} \end{pmatrix} - \begin{pmatrix} \phi \\ \alpha \\ \theta \\ \tilde{J} \end{pmatrix} = 0. \tag{4.12}$$

The idea of the proof is to show that equation (4.12) can be solved perturbatively in ε close to a periodic orbit of the circular case. Neglecting second order terms, Eq. (4.12) is rewritten as

$$(Df^m - \mathbb{1}) \begin{pmatrix} \phi - \phi_0 \\ \alpha - \pi \\ \theta - \theta_0 \\ \tilde{J} - \tilde{J}_0 \end{pmatrix} + \varepsilon \frac{\partial f_\varepsilon^m}{\partial \varepsilon} = 0. \tag{4.13}$$

Here, Df^m is the derivative of the map at $\varepsilon = 0$ and $\frac{\partial f_\varepsilon^m}{\partial \varepsilon}$ is the derivative of the map with respect to ε, evaluated at $\varepsilon = 0,\ \phi = \phi_0,\ \alpha = \pi,\ \theta = \theta_0$ and $\tilde{J} = \tilde{J}_0$.

Due to the conservation of the Jacobi integral for the circular case, all matrix elements of the last row of $(Df^m - \mathbb{1})$ are equal to zero. In order to fulfill equation (4.13), the last row of the vector $\frac{\partial}{\partial \varepsilon} f_\varepsilon^m$ must therefore be equal to zero. This is indeed the case for most of the perturbations as it is shown in Appendix C, where Appendix B was used to calculate the derivative of f_ε^m. Especially, this is true for the movement on a keplerian ellipse. So the number of linear equations is reduced by one. In addition, for the circular case, the dependence on ϕ is trivial. Then, the system of linear equations has the form

$$\mathbf{B}(m) \begin{pmatrix} \alpha - \pi \\ \theta - \theta_0 \\ \tilde{J} - \tilde{J}_0 \end{pmatrix} = -\varepsilon \frac{\partial \hat{f}_\varepsilon^m}{\partial \varepsilon}. \tag{4.14}$$

Here, the matrix $\mathbf{B}(m)$ is given by the matrix $(Df^m - \mathbb{1})$, where the first column and the last row is omitted, and $\hat{f}_\varepsilon^m$ represents the corresponding map.

For the existence of a solution of (4.14), the determinant of the matrix $\mathbf{B}(m)$ must be different from zero. The determinant can be written as

$$\det(\mathbf{B}(m)) = C\, m(\lambda^{m/2} - \lambda^{-m/2})^2, \tag{4.15}$$

where λ is the eigenvalue corresponding to the fixed point of the circular case and C is a constant which is independent of m (see Appendix D). The expression 4.15 can only be zero for $\lambda^m = 1$. Alternatively, from the expression for $\mathbf{B}(m)$ we obtain

$$\det(\mathbf{B}(1)) = -\frac{R\,\delta\phi^3}{d\,(R-d)^2\,\cos(\theta_0)^2} \tag{4.16}$$

(see Appendix A). This expression can only be zero if $\delta\phi$ is zero, i.e., if the angle difference between two successive bounces would be zero. Therefore, in the cases $\delta\phi = 0$ or $\lambda^m = 1$ one cannot continue the periodic orbits of the circular case to the perturbed case. Otherwise, the matrix $\mathbf{B}(m)$ can be inverted and the system of linear equations (4.13) has exactly one solution. This establishes that the fixed points of the circular map can be deformed for non–zero ε and yield periodic orbits of the perturbed case, except for the cases described in Appendix C.

4.3 The circular case

4.3.1 General considerations

In the circular case, the Jacobi integral (i.e., the Hamiltonian) [30, 33]

$$\tilde{J} = \frac{p_x^2 + p_y^2}{2} - (x\,p_y - y\,p_x) + V_d\left(\begin{pmatrix} R \\ 0 \end{pmatrix}, \vec{r}\right) \tag{4.17}$$

is a constant of motion, where the angular velocity ω was set to 1 here. The Jacobi integral can be written in the old coordinates having exactly the same analytical expression.

The Hamiltonian leads to the differential equations

$$\begin{pmatrix} \dot{x} \\ \dot{y} \\ \dot{p}_x \\ \dot{p}_y \end{pmatrix} = \begin{pmatrix} 0 & -1 & 1 & 0 \\ 1 & 0 & 0 & 1 \\ 0 & 0 & 0 & 1 \\ 0 & 0 & -1 & 0 \end{pmatrix} \begin{pmatrix} x \\ y \\ p_x \\ p_y \end{pmatrix}, \tag{4.18}$$

where the reflection has to be calculated separately.

The equation of motion without the reflection can be given analytically [31]

$$\begin{pmatrix} x \\ y \\ p_x \\ p_y \end{pmatrix} = \begin{pmatrix} \mathbf{D}(t) & t\,\mathbf{D}(t) \\ \mathbf{0} & \mathbf{D}(t) \end{pmatrix} \begin{pmatrix} c_1 \\ c_2 \\ c_3 \\ c_4 \end{pmatrix}, \tag{4.19}$$

where the matrix $\mathbf{D}(t)$ is given by

$$\mathbf{D}(t) = \begin{pmatrix} \cos(t) & -\sin(t) \\ \sin(t) & \cos(t) \end{pmatrix}. \tag{4.20}$$

N. Meyer *et al.* [30] have introduced the Poincaré map

$$(\alpha_{n+1}, \theta_{n+1}) = \mathcal{P}^1_{\tilde{J}}(\alpha_n, \theta_n), \tag{4.21}$$

which is not symplectic. The equation for the Jacobi integral (4.17) can be rewritten using the angles α, θ and the magnitude v of the velocity shortly after the bounce,

$$\tilde{J} = \frac{v^2}{2} - v\,(R\,\sin(\theta) + d\,\sin(\theta - \alpha)). \tag{4.22}$$

The equation (4.22) is quadratic in v. Therefore two solutions for v for a given Jacobi integral exist. It can be shown that for a positive value of the Jacobi integral only one positive solution exists. Thus, the Poincaré map (4.21) can be displayed in a θ vs. α plot. However for a negative Jacobi integral there are two positive solutions for v. If the Jacobi integral is equal to 0, $v = 0$ is always a solution. This has to be taken into account when plotting the Poincaré map (4.21).

Another Poincaré map is much more convenient because of its symplectic nature, as mentioned by Dullin [31]. For this Poincaré plot one uses the parallel to the surface of the disc component

$$p = -d - R\,\cos(\alpha) - v\,\sin(\alpha - \theta) \tag{4.23}$$

of the velocity $\vec{v}$ minus the vector potential $\vec{A} = (-y, x)^T$ and the angle α. The Poincaré map

$$(\alpha_{n+1}, p_{n+1}) = \mathcal{P}'_{\tilde{J}}(\alpha_n, p_n),\ \alpha \in \{0, 2\,\pi\} \text{ and } p \in \{-p_{max}, p_{max}\} \tag{4.24}$$

is symplectic and has the advantage to be one to one even for negative Jacobi integral and the definition domain can be given easily with
$p_{max} = \sqrt{2\,\tilde{J} + R^2 + d^2 + 2\,R\,d\,\cos(\alpha)}$.

4.3.2 Periodic orbits

The primitive periodic orbits or fixed points form the skeleton of the scattering dynamics. The orbits which reflect radially are fixed points of the map (4.21) [30]. When the projectile is reflected radially, the kinetic energy of the projectile remains constant. One has to calculate the velocity of the projectile such that the next reflection is radial. In this case, the velocity is

$$v = -2\frac{\cos\theta}{\delta\phi}(R - d), \tag{4.25}$$

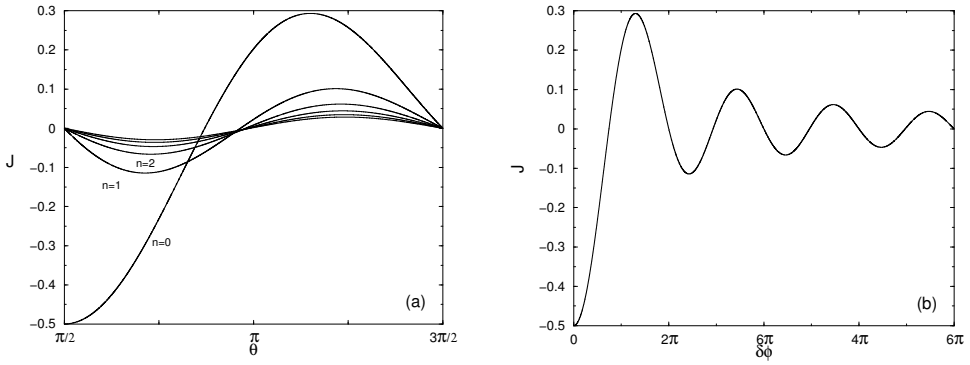

Figure 4.2: Jacobi integral for the fixed points of the circular case as a function of (a) θ and (b) $\delta\phi$.

where $\delta\phi$ is the angle difference between two successive bounces and is given by

$$\delta\phi = 2\,\theta + (2\,n - 1)\,\pi, \tag{4.26}$$

where $n \in \mathbb{N}^0$ denotes the number of full turns of the disc between successive bounces.

This shows that the periodic orbits can be parametrized by the angle θ and the number n. These values leads to the Jacobi integral [30]

$$\tilde{J}_n^{R,d} = (R-d)^2 \frac{2\cos(\theta)^2 + \delta\phi\,\sin(2\,\theta)}{\delta\phi^2} \tag{4.27}$$

for the fixed points. In the following, the scaled Jacobi integral

$$J = \frac{\tilde{J}}{(R-d)^2}, \tag{4.28}$$

where $\tilde{J}$ is the Jacobi integral (4.17), will always be used.

In Figure 4.2 (a) the plot of the Jacobi integral J_n vs. the angle θ is shown. There are different maxima and minima of the graph. These extrema are given by the equation [30]

$$0 = \delta\phi^2\,(1 - \tan^2(\theta)) - 4\,(1 + \delta\phi\,\tan(\theta)). \tag{4.29}$$

As mentioned above, two solutions for the velocity v for a negative value of the Jacobi integral exist. It is therefore possible that two periodic orbits exist with the same values for α, θ and J in Figure 4.2 (a). Note that these crossings are not bifurcations. Both periodic orbits still exist.

The variables α and θ are not canonical conjugate variables, but one can prove that for the special case of the fixed points of the non–symplectic Poincaré map (4.21) the determinant of the derivative is 1. If a two–dimensional map has a derivative with determinant 1 then the trace of the derivative gives the information of the characteristic multipliers of the orbit [13, 34, 35]. If the trace is of absolute value smaller than two, then the periodic orbit is elliptic. If it equals two, the periodic orbit is parabolic, if the absolute value of the trace is larger than 2, then the periodic orbit is hyperbolic. The trace of the derivative of both Poincaré maps is given by

$$Tr\, D\mathcal{P}_{\tilde{J}} = \frac{2\,\tilde{d} + (\delta\phi^2 - 4) - 4\,\delta\phi\,\tan(\theta) - \delta\phi^2\,\tan(\theta)^2}{\tilde{d}}, \tag{4.30}$$

where the notation $\tilde{d} = d/R$ is used.

In Figure 4.3, we show the trace as a function of the angle θ for a specific case of $\tilde{d}$.

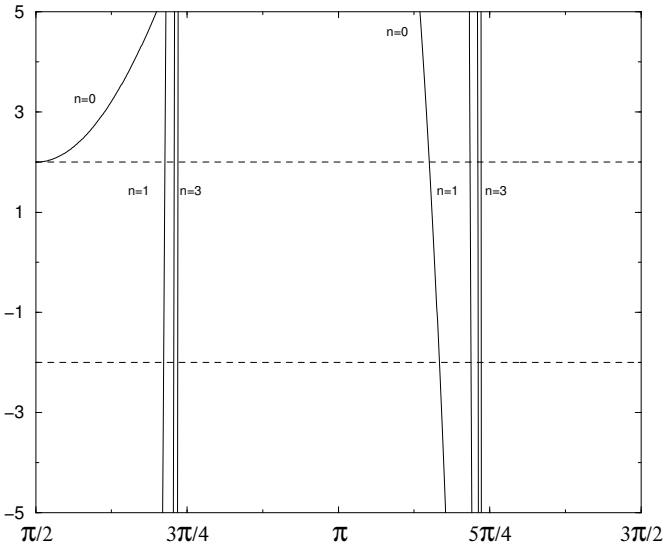

Figure 4.3: The trace of the derivative of the Poincaré map $\mathcal{P}_{\tilde{J}}$ for the circular case.

It is known that two–dimensional maps with the determinant of the derivative equal to 1, bifurcations can only occur if the characteristic multipliers are 1 or -1 [35]. This is equivalent to a trace of the derivative of 2 or -2. Setting the trace (4.30) to 2, the equation (4.29) is readily obtained. It is remarkable that this equation is independent of the radius $\tilde{d}$ of the disc. If the trace equals to -2 the equation

$$0 = \delta\phi^2 + 4\,\tilde{d} - 4 - 4\,\delta\phi\,\tan(\theta) - \delta\phi^2\,\tan^2(\theta) \tag{4.31}$$

must be fulfilled.

It can be shown that for large n the created elliptic fixed point gets unstable before the next two fixed points are created (see Appendix E). Thus it seems that the map gets hyperbolic before the next two fixed points are born.

The case $J = 0$ must be considered separately. Then, due to the equation (4.28) the conditions

$$\theta = \frac{\pi}{2},\ \theta = \frac{3\,\pi}{2} \text{ or } -1 = \delta\phi\ \tan\theta \tag{4.32}$$

for the angle θ of the fixed points must be satisfied. The first and second equation (4.32) is valid for all n except for the case $n = 0$ and $\theta = \frac{\pi}{2}$.

For the first and the second condition (4.32) the velocity (4.25) of the periodic orbit is 0. The trace of the derivative of the Poincaré map of these fixed points can be calculated and are given by $Tr\,D\mathcal{P}_0 = -\infty$. In the symplectic Poincaré map (4.24) these periodic orbits are located at $p = (R - d)$ and $\alpha = \pi$, which is right on the boundary of the definition domain.

For the fixed points fulfilling the last condition of (4.32), the trace

$$TrD\mathcal{P}_0 = 2 + \frac{\delta\phi^2 - 1}{\tilde{d}} \tag{4.33}$$

is obtained. For $n = 0$, the third condition of (4.32) is satisfied by the angle $\theta^0 \approx 2.736$. For all other n, the angle, which satisfies the last condition of (4.32), is between θ^0 and π. The angle difference $\delta\phi$ will always be greater than one. Thus the trace (4.33) will be greater than two and therefore these fixed points are all hyperbolic. Additionally, this family of periodic orbits has an accumulation point at $\alpha = \pi$ and $p = (R - d)$ in the symplectic Poincaré map (4.24).

4.3.3 Bifurcation scenario

We assume in the following that the system gets hyperbolic before the next homoclinic intersection occurs. This could not be shown for all $\tilde{d}$, but this assumption seems to be reasonable because the elliptic fixed point gets inverse hyperbolic long before the next saddle–center bifurcation occurs (see Appendix E). Additionally, the magnitude of the eigenvalues of the linearized map are very big when the next saddle–center bifurcation occurs and one can easily imagine the bifurcations scenario for the other cases.

With the above assumption the following bifurcation scenario is obtained. A schematic view is shown in Figure 4.4 and 4.6. The bifurcation scenario can also be seen in the Poincaré maps of the symplectic map (4.24) in Appendix F.

First, the bifurcation scenario for positive Jacobi integral is explained. We indicate by J_n^{max} the maximum of the Jacobi integral for J_n. The value of the Jacobi integral for which one has a $2\,n+2$ complete binary horseshoe map is denoted by J_n^c. Finally, J_n^h belongs to the first appearance of homoclinic intersections of the tendril, which folds back, with the fundamental region. The complete hyperbolic horseshoe has $n+1$ hyperbolic and $n+1$ inverse hyperbolic fixed points.
If the Jacobi integral is bigger than J_0^{max} in Figure 4.2 then no periodic orbits exist. If one reduces the value of the Jacobi integral then a saddle–center bifurcation occurs at J_0^{max} and two fixed points are created. This is an incomplete binary horseshoe. Decreasing the Jacobi integral further leads to a series of period–doubling bifurcation until a complete binary horseshoe is reached at J_0^c. This scenario is shown in Figure 4.4 (a) and (b). The square indicates the fundamental rectangle of the scattering given by the stable and unstable manifold of the outer fixed point. The shaded area indicates how the fundamental rectangle gets distorted under the map f.
A further decrease of the Jacobi integral stretches the tendrils until they reach the boundary. Afterwards they reappear at the other side of the domain. This discontinuinity of the stable resp. unstable manifold arises, because the transversality of the Poincaré map is violated. In Figure 4.5 two trajectories in the rotating coordinate system are shown. One trajectory belongs to the unstable manifold before the discontinuity and the other trajectory to the unstable manifold just after the discontinuity. The orbits just after the discontinuity just does not hit the disc and makes an additional loop. By reducing the Jacobi integral even more, the tangle gets folded back until it reaches the fundamental rectangle at J_1^h. The tangle hits the fundamental rectangle as indicated in Figure 4.4 (c). Afterwards, the tendril in Figure 4.4 (c) will cross the fundamental rectangle and create at J_2^{max} the two fixed points. By further decreasing the Jacobi integral one finally arrives at J_2^c, where the dynamics is given by a complete quarternary horseshoe map.
The same scenario with folding back of the tendril in the middle of the big gap and a subsequent saddle–center bifurcation repeats itself. It should be clear from the above scenario that all inverse hyperbolic fixed points are on the right–hand side of the normally–hyperbolic fixed points in the schematic graphs in Figure 4.4.

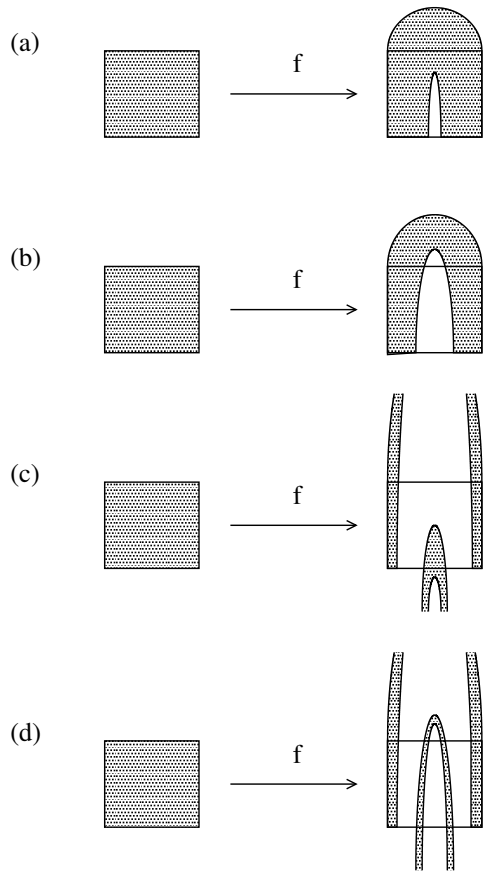

Figure 4.4: Bifurcation scenario for the circular case and positive Jacobi integral, if
(a) $J_0^{max} > J > J_0^c$,
(b) $J_0^c > J > J_1^h$,
(c) $J_1^h > J > J_1^{max}$,
(d) $J_1^c > J > J_2^h$.

Nearly the same notation as above will be used for the case of negative Jacobi integral, but all values of the Jacobi integral will be denoted by a prime, and instead of the maximum, the minimum of the Jacobi integral has to be taken. The hyperbolic case at $J_n^{c'}$ is a $2\,n+1$ horseshoe map with $n+1$ hyperbolic and n inverse hyperbolic fixed points, except for the case $n = 0$.
For a Jacobi integral smaller than -0.5, the map has no fixed points. Then one fixed point arises which is first neutral but gets hyperbolic quickly. The stable and unstable manifold have no homoclinic intersections. By increasing the Jacobi integral, the stable and unstable manifold gets discontinuous and enters at the other

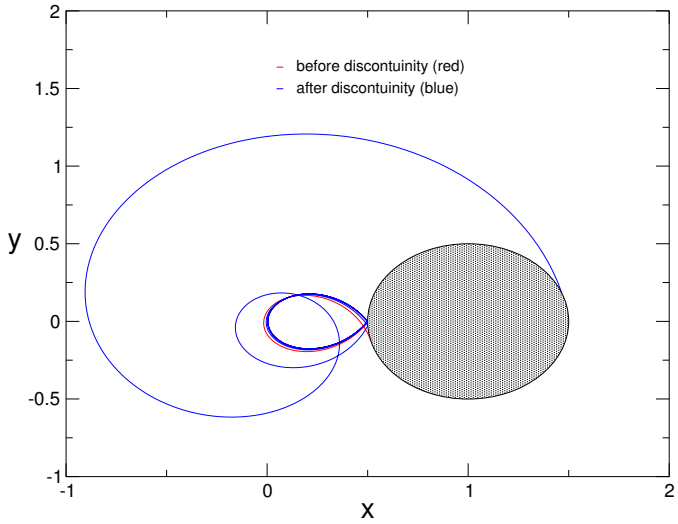

Figure 4.5: The transversality violation

side of the domain, similar to the case of positive Jacobi integral. By further increasing the Jacobi integral, one gets the first homoclinic point at $J = J_1^{h'}$. The map corresponds to a horseshoe map in higher iterates. If one increases the Jacobi integral more, the tendrils of the stable and the unstable manifold finally meet each other at $J < J_1^{min'}$. This case is shown in Figure 4.6 (a) and corresponds to an incomplete ternary horseshoe. By increasing the Jacobi integral further, one reaches the value $J_1^{min'}$, where through a saddle–center bifurcation, two fixed points arise and the ternary horseshoe is still incomplete. One reaches the complete ternary horseshoe case by further increasing the Jacobi integral at $J_1^{c'}$ (Figure 4.6 (b)). By a further increase of the Jacobi integral the tendril gets longer, hits the boundary, gets discontinuous through transversality violation, will be folded back, and hits the fundamental rectangle at $J_2^{h'}$ as in the positive Jacobi integral case. A case with $J_2^{h'} < J < J_2^{min'}$ is shown in Figure 4.6 (c). If one increases the Jacobi integral more, a saddle–center bifurcation occurs at $J_2^{min'}$ and one reaches finally a complete quintuple horseshoe at $J_2^{c'}$ (see Figure 4.6 (d)). This scenario repeats itself as in the positive Jacobi integral case.

Similar to the positive Jacobi integral case all normally–hyperbolic fixed points are on the right hand side of the inverse hyperbolic fixed points in the schematic graphs in Figure 4.4.

In Figure 4.7, we show the first two applications of the symplectic Poincaré map on the yellow area, which is approximately the fundamental region for $J = 0$. The boundary of the domain is indicated by the blue line. The fundamental region is given by the stable and the unstable manifold of the fixed point for $n = 0$. The results for periodic orbits (see section 4.3.2) give evidence that the bifurcation from

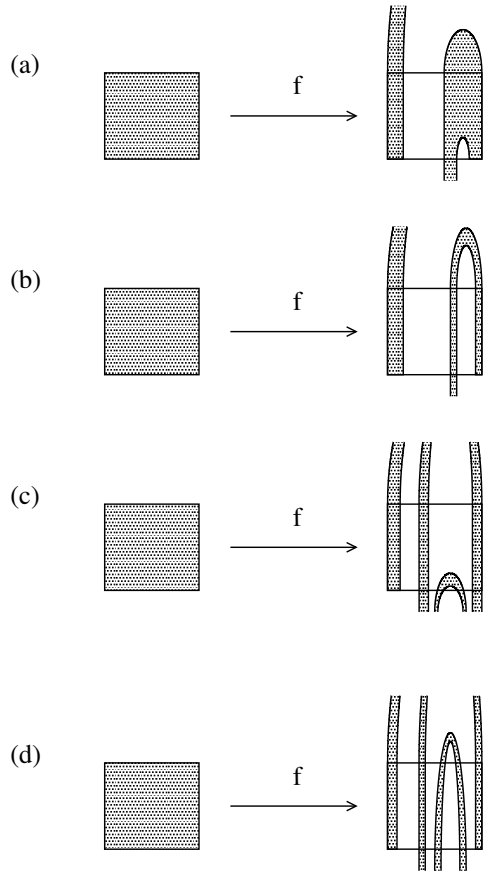

Figure 4.6: Bifurcation scenario for the circular case and negative Jacobi integral, if
(a) $J_1^{h'} < J < J_1^{min'}$,
(b) $J_1^{c'} < J < J_2^{h'}$,
(c) $J_2^{h'} < J < J_2^{min'}$,
(d) $J_2^{c'} < J < J_3^{h'}$.

positive (or negative) Jacobi integral to $J = 0$ occurs in the way described below. All inverse hyperbolic fixed points merge to one inverse hyperbolic fixed point with velocity 0 which is infinitely unstable with $p = R - d$ and is located right on the boundary of the domain. The horseshoe has infinitely many normal hyperbolic fixed points with maybe one inverse hyperbolic fixed point. The inverse hyperbolic fixed point lies on the boundary and we believe that it also lies on the boundary of the fundamental rectangle. Thus we think that it is a completely hyperbolic horseshoe with infinitely many hyperbolic and one inverse hyperbolic fixed points.

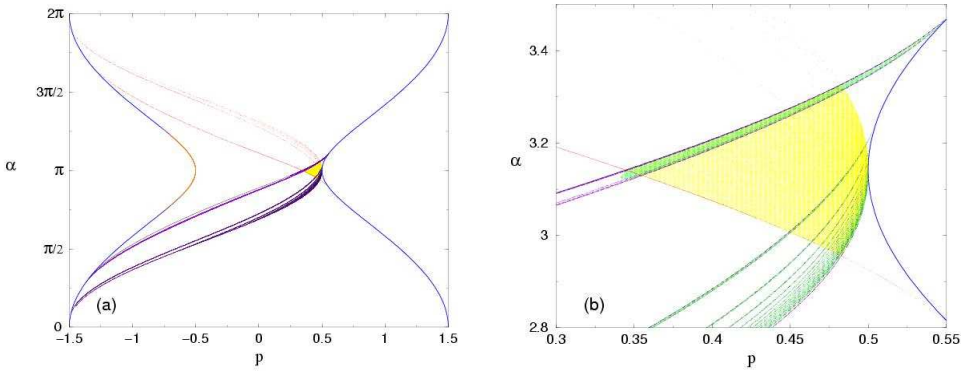

Figure 4.7: (a) The Poincaré map of the case $J = 0$. The stable manifold is in red and the unstable in black. The approximated fundamental rectangle is yellow and the first resp. the second iterate of the fundamental region are green resp. violet points. Additionally, the boundary of the domain is shown in blue and some whispering gallery orbits in orange. (b) A magnification of the fundamental domain.

An explanation why there is an even number of fixed points for $J > 0$ and an odd number of fixed points for $J < 0$ can be seen in Figure 4.2 (b). The inverse hyperbolic fixed points with a positive Jacobi integral J_n corresponds to the inverse hyperbolic fixed points with negative Jacobi integral J_{n+1}. Additionally, there is no inverse hyperbolic fixed point which belongs to J_0.

The derivative of the periodic orbits for the 4D symplectic map proposed by Dullin [31] is shown in Appendix G. One eigenvector for the eigenvalue 1 can by seen easily. The corresponding Krein signature is 0, so bifurcations with four eigenvalues equal to 1 to eigenvalues $\lambda, 1/\lambda, \overline{\lambda}, 1/\overline{\lambda}$ can occur.

4.3.4 Simulations

We now present simulations for the circular case to better understand the higher–dimensional cases.

In the following graphs the initial conditions with a minimal number of bounces are shown. The initial angle α was kept fixed at π if not indicated otherwise. To draw conclusions from the plots one should be aware that elliptic and parabolic regions and the stable manifold with an initial angle $\alpha = \pi$ are visible.

In Figure 4.8 the magnitude of the velocity vs. the angle θ is shown. It must be said that the Jacobi integral is not fixed here. The same graph, but the scaled Jacobi integral J (4.28) vs. the angle θ is shown in Figure 4.9.

In the plot 4.9 some strange cuts are seen, they are due to the fact that this graph was obtained by a transformation applied to Figure 4.8 and so the straight boundary in the Figure 4.8 is not straight, here. All plots with the Jacobi integral were obtained in this way, so in all of these plots some parts are distorted (but can be identified easily).

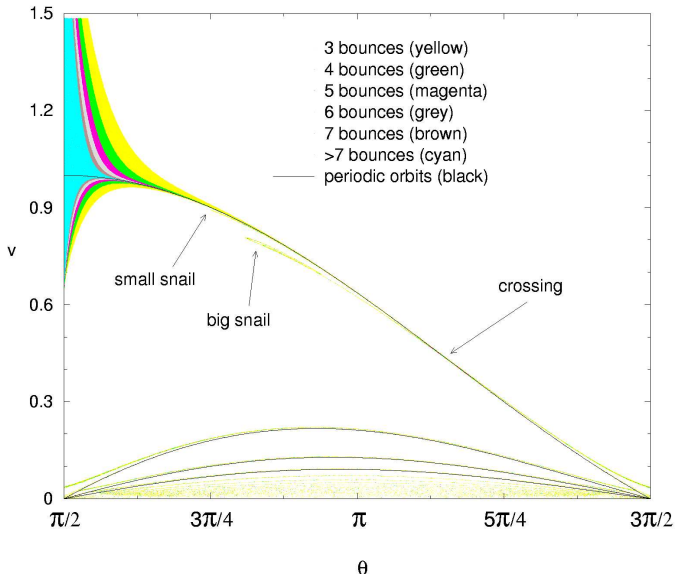

Figure 4.8: The velocity vs. the angle θ.

In both Figures the periodic orbits are drawn as black lines. There are different regions which catch the eye. The big part with a lot of bounces in the left upper corner of Figure 4.8 can clearly be identified as whispering gallery orbits. They correspond to the left lower part in Figure 4.9.

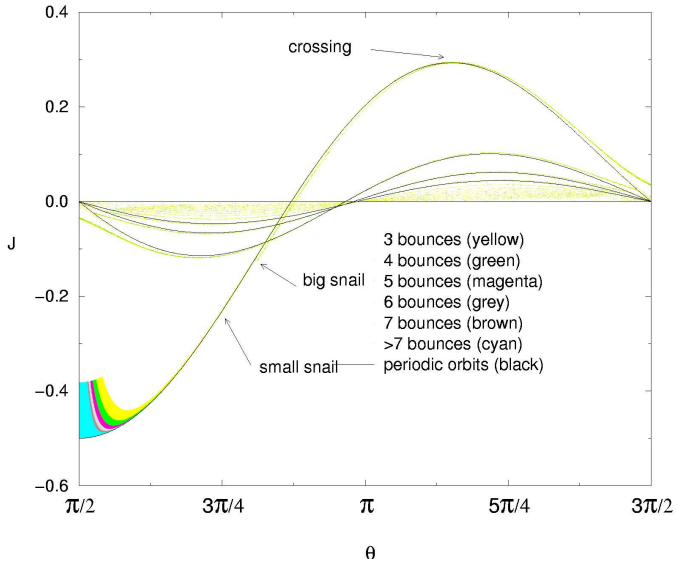

Figure 4.9: The Jacobi integral vs. the angle θ.

The place which was called crossing by J. Broch in his Diploma thesis is due to the first bifurcation for positive Jacobi integral. This can clearly be seen in Figure 4.9 and the magnification of this region in Figure 4.10. At the place where the second bifurcation occurs, a similar picture is seen, except that there is no crossing (which is clear from the bifurcation scenario in section 4.3.3).

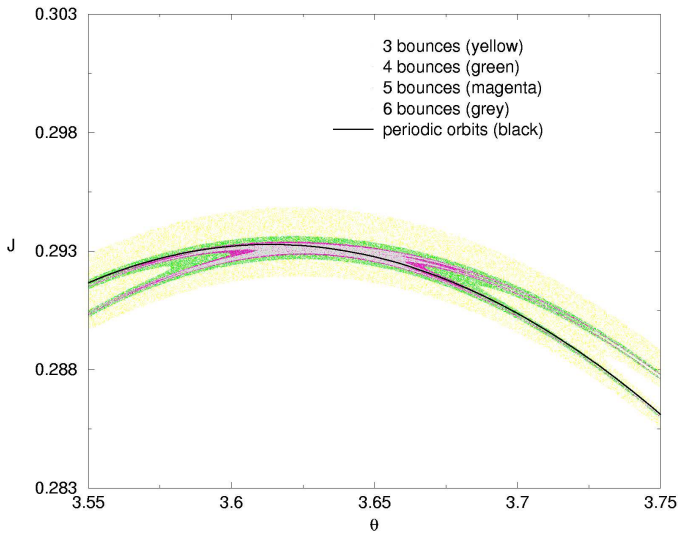

Figure 4.10: A magnification of the crossing in the Jacobi integral vs. θ.

A magnification of the big snail in the v vs. θ plot is shown in Figure 4.11 (a). In

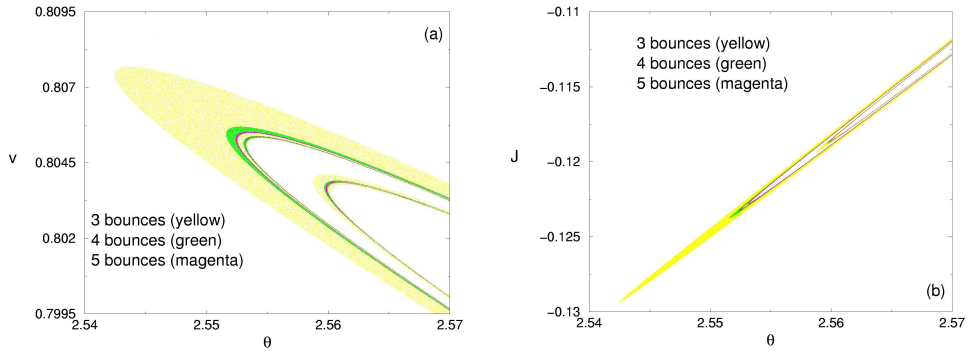

Figure 4.11: (a) A magnification of the big snail in the v vs. θ plot and (b) the Jacobi integral vs. θ plot.

Figure 4.11 (b) the corresponding plot in the Jacobi integral vs. θ plane is shown. In Figure 4.12, a Poincaré plot of the symplectic map and a magnification around the outer fixed point near the first homoclinic intersection for a negative value of the Jacobi integral is shown. The stable manifold is plotted in red, the unstable manifold in black, the border of the definition domain in blue and the $\alpha = \pi$ line in green.
After the bifurcation scenario for every n a tendril folds back in the gap of the tendril 1 and therefore also in every small tendril (tendril 2, 3, ...). In this way loops are formed and the "snail" structure is generated, since every crossing of a tendril with the $\alpha = \pi$ line is seen as a loop in these plots. In Figure 4.12 a Poincaré plot is shown for a case, where the tendril 2 just does not cross the $\alpha = \pi$ line, in contrast to the first iterate of tendril 2 (tendril 3). In Figure 4.13, the Jacobi integral is increased and thus the tendril 2 is stretched more and has just crossed the line $\alpha = \pi$. Therefore a loop is seen in Figures 4.11.

Thus the big snail is due to the intersection of the tendril 2 with the $\alpha = \pi$ line, whereas the tendril 3 leads to the small snail structure.

The above considerations about the snail structures show that for every iterate of the tendril 2 such a "snail" exists and every iterate is closer to the fixed point in every plot. Additionally, every higher iterate must be seen at a lower value of the Jacobi integral.
A closer look at the plot 4.9 shows, that over resp. under every maximum resp. minimum of the periodic orbits line, an ensemble with more than three bounces is seen. A closer investigation leads to the conclusion that this is the folding back of the tendril 1 in the above Poincaré plots. Because for every n a tendril folds back and leads finally to the saddle–center bifurcation, such loops can be seen over resp. under every periodic orbits line in the plot. An example is shown in Figure 4.14. One loop is from the periodic orbits and the others are from the folding of

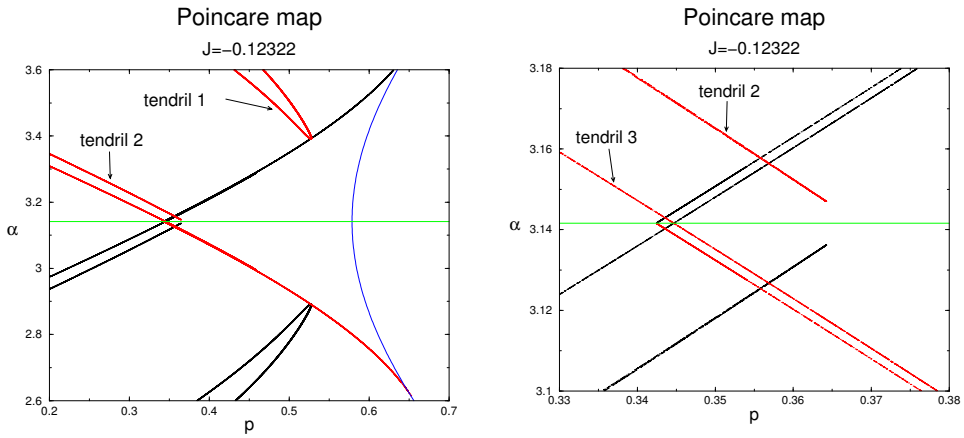

Figure 4.12: In these Poincaré plots the stable manifold is red and the unstable manifold is black. Additionally, the border of the definition domain (blue) and the line $\alpha = \pi$ (green) is shown.

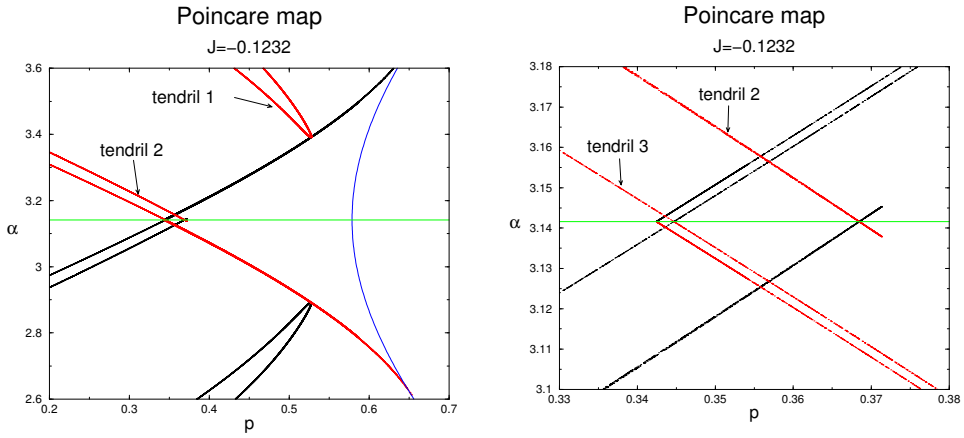

Figure 4.13: Poincaré plot is for a further value of J, where the same colours as in Figure 4.12 were used.

the stable manifold.

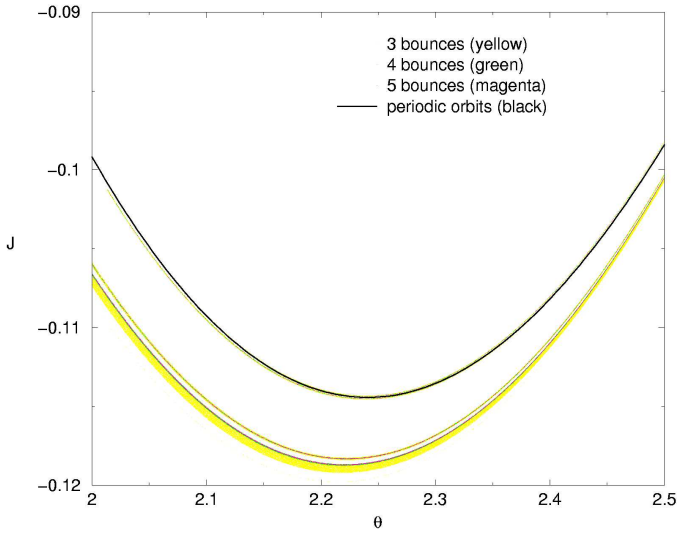

Figure 4.14: A magnification of the loops around the periodic orbits in the Jacobi integral vs. θ plane.

Thus every detail of Figure 4.8 is understood.

The general considerations are also correct for higher–dimensional maps. Thus if some "snail" structure is present in such plots, then this is due to some homoclinic or heteroclinic intersections.

In Figure 4.15, the same plots are shown as in Figure 4.8, but with different initial angle α and the ensemble with at least 3 bounces is shown. Obviously the plots change dramatically. This is because there are no fixed points with initial angle $\alpha \neq \pi$ and thus only some intersections of the stable manifold are seen. Because the stable manifold folds down to a smaller angle of α, as can be seen in Figure 4.12, there are no intersections of the $\alpha = 0.9\,\pi$ line with the stable manifold, in contrast to the line $\alpha = 1.1\,\pi$, where such intersections exists. This can be seen in Figure 4.15 where no orbits with more than 2 bounces exist for $v < 0.3$ and $\alpha = 0.9\,\pi$. It should be mentioned that the Poincaré maps in Appendix F are for another case of $\tilde{d}$ as in these simulations.

In Figure 4.16 the results of escape rate simulations are shown. The logarithm of the number of orbits with a certain amount of bounces vs. the number of the bounces resp. the logarithm of the number of bounces are shown. If there are no orbits with a certain amount of bounces in Figure 4.16 we have set the logarithm to -1 for graphical reasons. In Figure 4.16 (a), the map is completely hyperbolic and

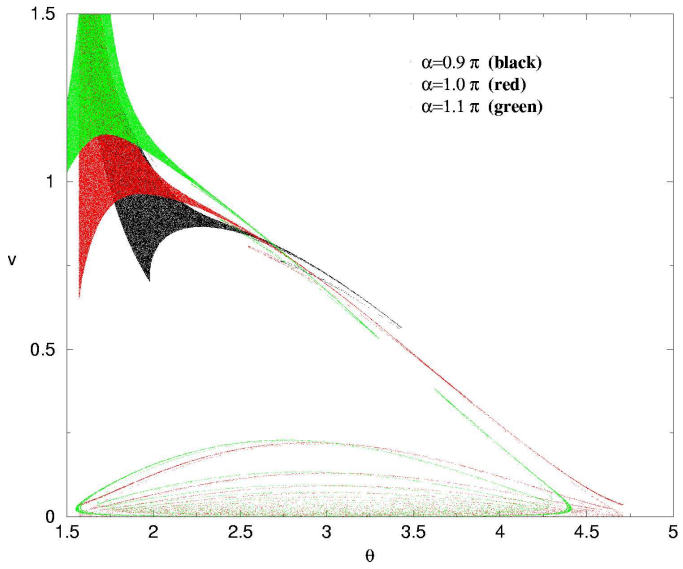

Figure 4.15: The ensemble of initial conditions with at least 3 bounces in the v vs. θ plane with different initial angle α.

corresponds to a complete binary horseshoe. Note that the exponential decay law for the escape can be seen.

In Figure 4.16 (b), the escape rate for a distribution of the initial conditions around a stable island is shown. Here the Jacobi integral is not constant in contrast to Figure 4.16 (a). The escape rate can be fitted to an algebraic decay law with an exponent α of nearly 0.8. The relative amount of orbits with more than 100'000 reflections to orbits with 10'000-100'000 reflections are approximately 200 times higher than we would expect due to the exponent α. Thus one can conclude that there is a stable island in this region (see section 3.5).

In the Figure 4.17 orbits near the first maximum of the Jacobi integral which stays in the system for more than 1'000 bounces or approximately 600 periods of the disc are shown in the fixed frame. It can be seen that they form a big ring. This ring can be estimated if we plot the periodic orbits for the case when the trace is equal ± 2. The periodic orbit with angle θ and $t \in [0, \delta\phi]$ and the disc at $\phi = 0$ can be calculated as

$$\vec{h}(t) = (R - d)\,\vec{n}(t) + t\,\vec{n}(t - \theta)v. \tag{4.34}$$

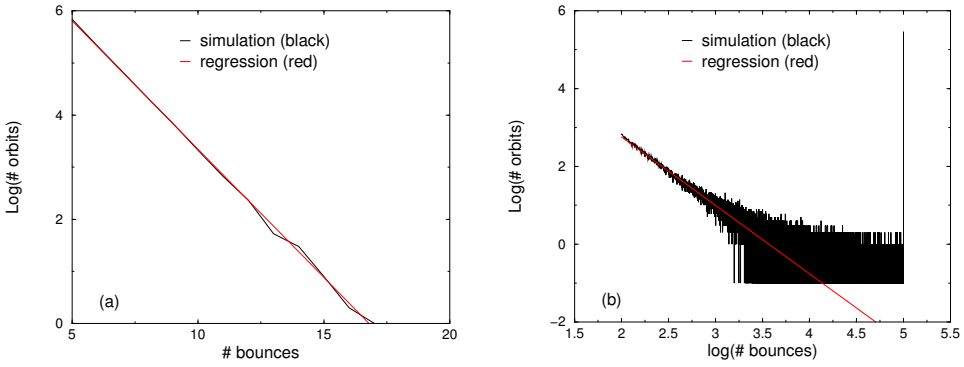

Figure 4.16: Escape law for the circular motion of the disc, for (a) a completely hyperbolic case and (b) for a case with an elliptic region.

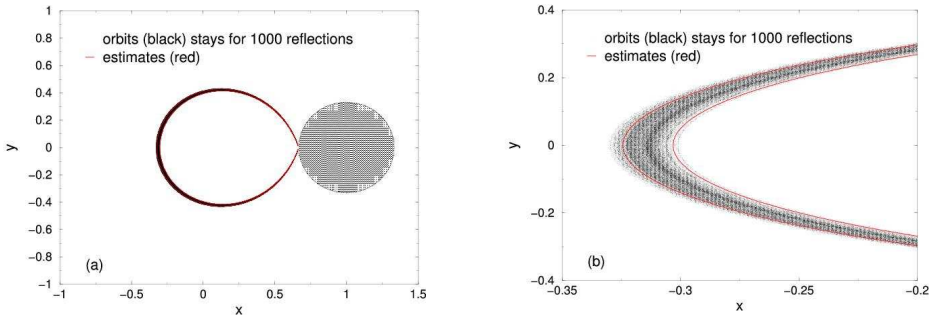

Figure 4.17: (a) The ring for the circular motion of the disc with the disc located at $\phi = 0$. (b) A magnification of the left hand side of the ring.

4.4 Non-circular orbit of the disc

4.4.1 General considerations

Due to the breaking of the symmetry the Jacobi integral is not a constant of motion anymore and thus the toy model leads to a 4D Poincaré map. The fixed points of the synodic frame are in the rest frame a whole family of periodic orbits with at least two neutral directions with eigenvalue 1 if the disc moves on a circular orbit. If the symmetry is broken, almost all periodic orbits still exists after section 4.2 and the two neutral directions can get unstable or stay neutral (see section 2.6). Now assume that the periodic orbit bounces n times before it gets closed. Then the characteristic multipliers are nearly $2\,\pi/n$ periodic in the angle ϕ, because the characteristic multipliers are unique.

4.4.2 The elliptic case

If the disc moves on a keplerian ellipse one can parameterize [36] the movement as

$$\vec{X}_R(\phi) = \frac{1-\varepsilon^2}{1+\varepsilon\cos(\phi(t))}\vec{n}(\phi(t)). \tag{4.35}$$

The movement was defined that the period is equal $2\,\pi$ for all eccentricities.
Then the derivative of the angle ϕ is given by

$$\dot{\phi} = \frac{(1+\varepsilon\,\cos(\phi))^2}{(1-\varepsilon^2)^{3/2}}. \tag{4.36}$$

This leads to an implicit function for $\phi(t)$,

$$t\,(\phi) = \sqrt{1-\epsilon^2}\left[\frac{2}{\sqrt{1-\epsilon^2}}\arctan\frac{(1-\epsilon)\tan\frac{\phi}{2}}{\sqrt{1-\epsilon^2}} - \frac{\epsilon\sin\phi}{1+\epsilon\cos\phi}\right]. \tag{4.37}$$

The expressions (4.35) and (4.36) inserted in the Hamiltonian J_g (4.6) yields to the Hamiltonian

$$\begin{aligned} J_e &= \left(\vec{p}^2 - 2\sqrt{1-\varepsilon^2}\,(p_y\,x - p_x\,y) - \frac{2\,\varepsilon\sqrt{1-\varepsilon^2}\;<\vec{r},\vec{p}>\;\sin(\phi)}{(1+\varepsilon\,\cos(\phi))}\right) \\ &\quad \times\frac{(1+\varepsilon\,\cos(\phi))^2}{2\,(1-\varepsilon^2)^2} \end{aligned} \tag{4.38}$$

for the disc moving on a keplerian ellipse.

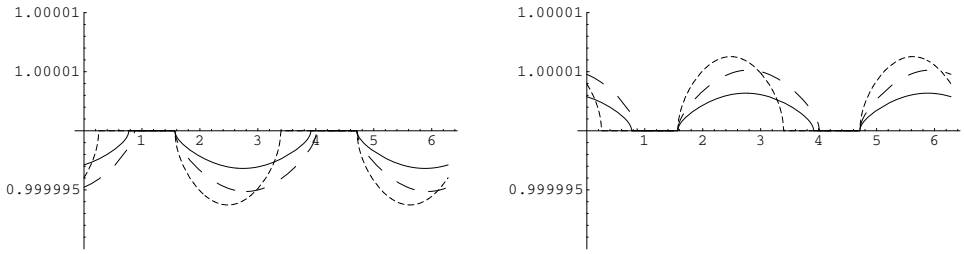

Figure 4.18: The ϕ–dependence of the magnitude of the characteristic multipliers corresponding to the neutral directions of the periodic orbits with two bounces are shown. The radius of the disc d is increased from the short–dashed to the solid to the long–dashed line.

For small eccentricities the periodic orbits can be calculated by using the method in section 4.2. As an example the periodic orbits with two bounces are calculated in the Appendix H.

The characteristic multipliers of this periodic orbits of the non-symplectic Poincaré map

$$P_\varepsilon \begin{pmatrix} \phi_{n+1} \\ \theta_{n+1} \\ \alpha_{n+1} \\ J_{n+1} \end{pmatrix} = f_\varepsilon \begin{pmatrix} \phi_n \\ \theta_n \\ \alpha_n \\ J_n \end{pmatrix} \tag{4.39}$$

were calculated by using the second derivatives. The second derivatives could be obtained as mentioned in the Appendix A. The two non-neutral directions have no ϕ–dependence in first order. The dependence of the magnitude of the other two eigenvalues are shown in Figure 4.18, where the radius d of the moving disc is increased from the short–dashed to the solid to the long–dashed line.

It is interesting that the periodic orbits for some radii gets more unstable if the radius d of the disc is increased.

4.4.3 Simulations

The main focus of the simulation, presented in this section is the search for stable regions in phase space. In Figure 4.19, the regions with a certain amount of bounces are shown for the initial conditions $\phi = 0$, $\alpha = \pi$, and eccentricity $\varepsilon = 0.001$. There is no significant change in the structure compared to Figure 4.8 of the circular case. The calculation of the periodic orbit with two bounces and the symmetry seems to indicate that for $\phi = 0$ the periodic orbits still have an angle $\alpha = \pi$.

J. Broch has performed simulations for higher eccentricities and different movement of the disc. Because most of the periodic orbits still exist after a perturbation,

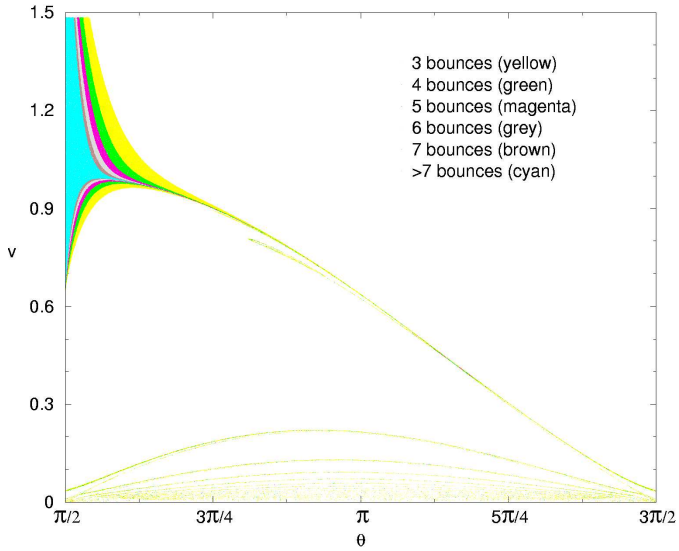

Figure 4.19: The velocity vs. the angle θ plotted for $\varepsilon = 0.001$.

the plot should not change dramatically if the disc moves on orbits close to a circular orbit. This expectations could be verified in those simulations.
In Figure 4.20 we show the projections of the initial conditions of orbits with more than 1'000 bounces close to the first saddle–center bifurcation in the circular case with $J > 0$. The dependence of the angle ϕ should not be too nasty for small eccentricity, such that nothing like folding back should occur.

In Figure 4.21, the approximated phase space volume of the above orbits vs. the angle ϕ is shown. A very fast reduction with increasing eccentricity and a strong dependence on the angle ϕ for high eccentricity can be seen.

The escape–rate simulations were made for the cases $\varepsilon = 0$, $\varepsilon = 0.001$, $\varepsilon = 0.0015$, $\varepsilon = 0.00165$ and $\varepsilon = 0.0017$ in the region of the phase space where the first saddle–center bifurcation occurs for $J > 0$. In all simulations, only orbits with more than 100 bounces are used. The regression is normally made using the orbits with 100 to 1'000 bounces, except for the case $\varepsilon = 0.0015$ where orbits with 200-1'000 bounces are used. The results are shown in the table 4.1. For the case $\varepsilon = 0.0017$, no orbits with more than 3'600 bounces were found. In Figure 4.22, the results of two of the above cases are shown. We have set the logarithm of the number of the orbits equal to -1 if no orbits with this amount of bounces where found. In Figure 4.22 (a) the eccentricity is $\varepsilon = 0.00165$. The high peak at the cut–off of the distribution is clearly visible which indicates the stable islands (see section 3.5). In Figure 4.22 (b), the eccentricity is $\varepsilon = 0.0017$. It is believed that no stable island exists in this phase space volume.

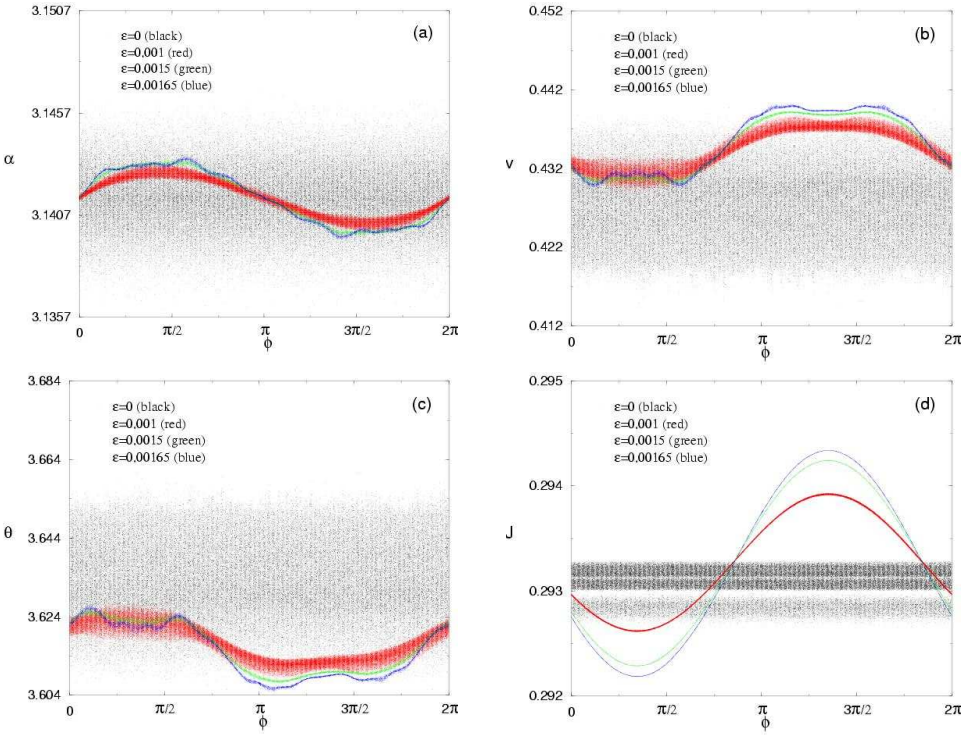

Figure 4.20: Projections of the approximated stable region for different eccentricities of the elliptic motion. Projection on the plane (a) α vs. ϕ, (b) v vs. ϕ, (c) θ vs. ϕ and (d) J vs. ϕ.

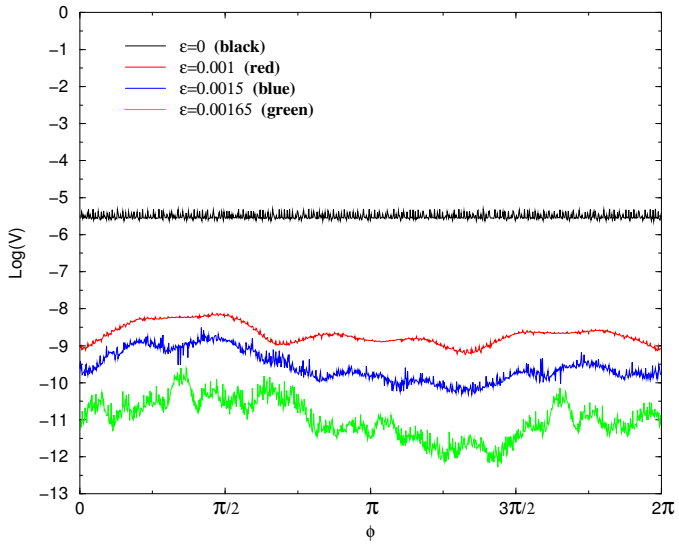

Figure 4.21: The logarithm of the approximated phase space volume V of the stable island for different eccentricities.

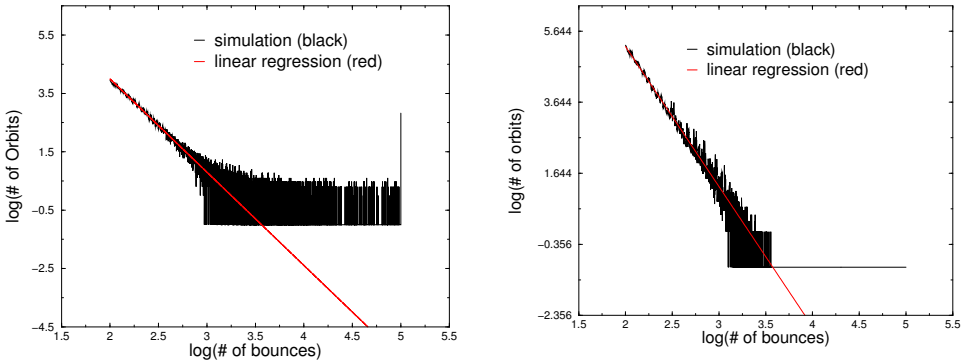

Figure 4.22: The differential escape–rate for the case (a) $\varepsilon = 0.00165$ and (b) $\varepsilon = 0.0017$. The results of the simulation are shown in black, the results of the linear regression in red.

ε	$\alpha - 1$	N	h
0	-1.8	0.77	267
0.001	-2.0	0.15	60
0.0015	-2.8	0.04	255
0.00165	-3.2	0.0015	237
0.0017	-3.9	0	0

Table 4.1: N is the fraction of orbits with more than 100'000 bounces, q is the quotient of the number of orbits with more than 100'000 bounces to the number of orbits with 10'000-100'000 bounces and $h = q/q_{reg}$, where q_{reg} is the value of q obtained from the regression. α is the exponent of the decay law (3.3).

In Figure 4.23 the projectiles which stay in the system for more than 1'000 bounces are shown for the eccentricity $\varepsilon = 0.00165$ in the rest frame. It is interesting that the ring is still complete but that a gap arises in the middle of it.

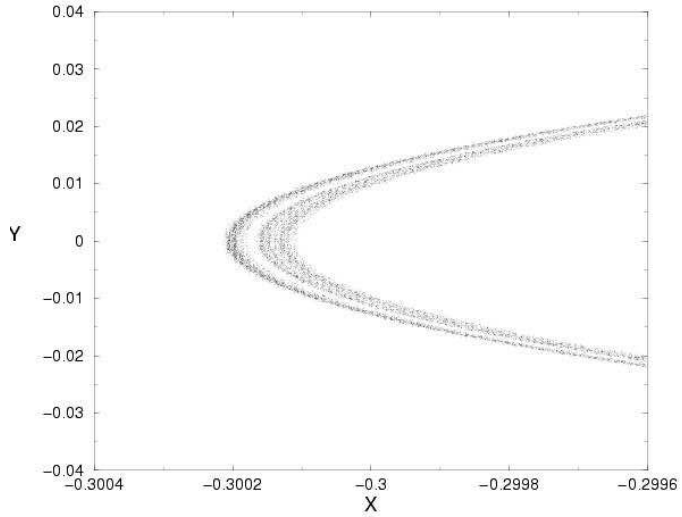

Figure 4.23: A magnification of the ring for an eccentricity of $\varepsilon = 0.00165$. The projectiles stay in the system for at least 1'000 reflections or approximately 600 periods.

Chapter 5

Conclusions and outlook

We have studied the dynamics of scattering on a hard disc which moves either on a circular orbit or on an elliptic keplerian orbit. Our studies are based on simulations and analytical calculations.

If the disc moves on a circular orbit a constant of motion exists and therefore the system has two effective degrees of freedom. The dynamics of this case is nearly completely understood. One open question is if the system becomes hyperbolic for all $\tilde{d}$ before the next homoclinic intersection occur. This could be proven by calculating the periodic orbits of period two and using the Feigenbaum constant ≈ 4.6692 to obtain the accumulation point of the period–doubling sequences [35]. The second open question is if the dynamics for Jacobi integral $J = 0$ is given by a horseshoe with an infinite number of hyperbolic fixed points or if it is a horseshoe with an infinite number of hyperbolic fixed points and one inverse hyperbolic fixed point.

Some progress in interpreting two dimensional scattering charts are made. Snail like structures in these charts indicate homo– or heteroclinic bifurcations.

For the problem of scattering on a disc moving on an elliptic keplerian orbit, or the symmetry broken case with three effective degrees of freedom, this study should be considered as a starting point for future works. Due to the knowledge of the elliptic regions of the disc moves on a circular orbit, "elliptic" regions could be found if the disc moves on an elliptic orbit. The indications for the existence of this stable island in phase space for eccentricities greater than 0 are strong. The phase space volume of this stable island decreases very fast with increasing eccentricity. These results are quite important to explain the stability of narrow planetary rings [37, 38]. To pursue this problem the scattering with a $1/r$ potential could be studied with a disc moving on a circular orbit, or a full simulation of the restricted three–body problem could be done. The methods used in this work are also suitable for the study of the scattering with a $1/r$ potential. The full simulation of

the restricted three–body problem should be made with faster computers than were available for this work.

A major problem for higher dimensional scattering is still that a the proper definition of the barriers in phase space is not known. There are other methods to investigate scattering systems, like detecting the periodic orbits [39] or the thermodynamical formalism [23]. But these are strongly computer–power and memory consuming. Additionally, one cannot be sure that all periodic orbits are detected and the thermodynamical formalism only supplies information on the asymptotic behavior.

Appendix A

The derivatives for the periodic orbits

The derivative of the map

$$\begin{pmatrix} \phi_{n+1} \\ \theta_{n+1} \\ \alpha_{n+1} \\ \tilde{J}_{n+1} \end{pmatrix} = f_\varepsilon \begin{pmatrix} \phi_n \\ \theta_n \\ \alpha_n \\ \tilde{J}_n \end{pmatrix} \tag{A.1}$$

of periodic orbits can be calculated. This method has the advantage in comparison to the one from Dullin [31] that higher derivatives can be calculated in the same way. The angles α, θ and ϕ are defined in Figure 4.1. It should be clear from the definition above that all derivatives of the Jacobi integral except the derivatives with respect to the Jacobi integral and the eccentricity are zero. The derivatives with respect to the angle ϕ are all 0 except the angle itself which is 1. The perturbation is taken to be an elliptic orbit. It is no problem to adapt the calculation of the derivative to other perturbations. It has to be mentioned that the calculation is made in the rest frame.

To shorten and simplify the equations the following abbreviations are introduced. Firstly ϕ, θ, α resp. $\tilde{J}$ will be denoted by x_1, x_2, x_3 resp. x_4. As in section 4.3.2 the angle difference between two successive bounces

$$\delta\phi = 2\,x_2 + (2\,n - 1)\pi \tag{A.2}$$

and the velocity for the periodic orbits

$$v_0 = -2\frac{\cos(x_2)\,(R-d)}{\delta\phi} \tag{A.3}$$

are used.

The derivatives are calculated by introducing perturbations in the initial conditions dx_i and comparing the terms with the same order in the equations.

The movement of the disc on a keplerian orbit for small eccentricity is given approximately in first order by the expression (A.4... A.6), where $\vec{n}(x_1)$ denotes the normal vector given in equation (4.2).

$$\begin{aligned}
\vec{r}(x_1) &= R\,\vec{n}(x_1) + \varepsilon\, R\,\vec{g}(x_1) && \text{(A.4)}\\
t(x_1) &= 1 - 2\,\varepsilon\,\sin(x_1) && \text{(A.5)}\\
\vec{g}(x_1) &= -\frac{1}{2}\left(\begin{pmatrix} 1 \\ 0 \end{pmatrix} + \vec{n}(2\,x_1)\right) && \text{(A.6)}
\end{aligned}$$

Due to the perturbation the starting position is given by

$$\vec{r_0} = R\,\vec{n}(x_1'^0) + \varepsilon\, R\,\vec{g}(x_1'^0) + d\,\vec{n}(x_1'^0 + x_3'^0), \tag{A.7}$$

where the abbreviation

$$x'^0{}_i = x_i^0 + dx_i \tag{A.8}$$

was introduced.

The Jacobi integral

$$x_4^0 = \frac{v^2}{2} - (\vec{r}_0^{\,x}\, v\,\sin(x_1'^0 + x_2'^0) - \vec{r}_0^{\,y}\, v\,\cos(x_1'^0 + x_2'^0)) - dx_4 \tag{A.9}$$

has to be constant for the initial conditions, so there must be a change of the magnitude of the velocity

$$v = v_0 + \sum_{i=1}^{4} \Delta v_i\, dx_i + \varepsilon\,\Delta v_\varepsilon \tag{A.10}$$

due to the perturbation of the initial conditions. In the expression (A.9) the superscript ^{x} resp. ^{y} denotes the x resp. y component of the vector.

With this equations one gets the change of the velocity (A.11) ... (A.15), with the abbreviation (A.16).

$$\begin{aligned}
\Delta v_1 &= 0 && \text{(A.11)}\\
\Delta v_2 &= \Delta v\, v_0\,(R-d)\,\cos(x_2^0) && \text{(A.12)}\\
\Delta v_3 &= \Delta v\, v_0\, d\,\cos(x_2^0) && \text{(A.13)}\\
\Delta v_4 &= \Delta v && \text{(A.14)}\\
\Delta v_\varepsilon &= -R\, v_0\,\cos(x_1^0)\,\sin(x_2^0) && \text{(A.15)}\\
\Delta v &= \frac{1}{v_0 - \sin(x_2^0)\,(R-d)} && \text{(A.16)}
\end{aligned}$$

The angle ϕ, where the projectile in the perturbed system hits the disc is given by

$$x_1^1 = x_1'^0 + \delta\phi + \sum_{i=1}^{4} \Delta\phi_i \, dx_i + \varepsilon \, \Delta\phi_\varepsilon. \tag{A.17}$$

At the reflection point the equation

$$d^2 = \left(\vec{r}_0 + v \, \vec{n} \left(\sum_{i=1}^{2} x_i'^0 \right) \left(x_1^1 - x_1'^0 + \varepsilon \left(t(x_1^1) - t(x_1'^0) \right) \right) - \vec{r}(x_1^1) \right)^2 \tag{A.18}$$

has to be fulfilled.
This equation leads to the derivatives (A.19) ... (A.23).

$$\frac{\partial x_1}{\partial x_1} = \Delta\phi_{x_1} = 1 \tag{A.19}$$

$$\frac{\partial x_1}{\partial x_2} = \Delta\phi_{x_2} = \frac{\delta\phi \, \left(\delta\phi \, \Delta v_2 - 2 \, (R-d) \, \sin(x_2^0) \right)}{2 \, (R-d) \, \cos(x_2^0)} \tag{A.20}$$

$$\frac{\partial x_1}{\partial x_3} = \Delta\phi_{x_3} = \frac{\delta\phi \left(\delta\phi \, \Delta v_3 - 2 \, d \, \sin(x_2^0) \right)}{2 \, (R-d) \, \cos(x_2^0)} \tag{A.21}$$

$$\frac{\partial x_1}{\partial x_4} = \Delta\phi_{x_4} = \frac{\delta\phi^2 \, \Delta v_4}{2 \, \cos(x_2^0) \, (R-d)} \tag{A.22}$$

$$\begin{aligned} \frac{\partial x_1}{\partial \varepsilon} = {} & \left(\delta\phi^2 \, \Delta v_\varepsilon - 2 \, \delta\phi \, R \sin(x_1^0) \, \sin(x_2^0) \right. \\ & \left. + 8 \, (d-R) \, \cos(x_2^0)^2 \, \sin(x_1^0 + x_2^0) \right) \times \frac{1}{2 \, \cos(x_2^0) \, (R-d)} \end{aligned} \tag{A.23}$$

The derivatives of α can be calculated by using the solutions for the derivatives of the angle ϕ (A.19...A.23) and the equation

$$\vec{x}_e = \frac{\vec{r}_0 + v \, \vec{n} \left(\sum_{i=1}^{2} x_i'^0 \right) \left(x_1^1 - x_1'^0 + \varepsilon \left(t(x_1^1) - t(x_1'^0) \right) \right) - r(x_1^1)}{d}. \tag{A.24}$$

The equation (A.24) gives the change of the cosine of the angle $\alpha + \phi$, but the derivative of α can be calculated by

$$\frac{\partial x_3}{\partial x_i} = \frac{-\frac{\partial \vec{x}_e^x}{\partial x_i}}{\sin(x_1^0 + 2\, x_2^0)} - \frac{\partial x_1}{\partial x_i}. \tag{A.25}$$

The derivatives are shown in the equations (A.26 ... A.29).

$$\frac{\partial x_3}{\partial x_2} = \frac{\delta\phi^2 \, \Delta\phi_2}{2 \, d \, \cos(x_2^0)} + \frac{(d-R) \, \left(2 + \delta\phi \, \tan(x_2^0) \right)}{d} \tag{A.26}$$

$$\frac{\partial x_3}{\partial x_3} = \frac{\delta\phi^2\,\Delta\phi_3}{2\,d\,\cos(x_2^0)} - \delta\phi\,\tan(x_2^0) - 1 \tag{A.27}$$

$$\frac{\partial x_3}{\partial x_4} = \frac{\delta\phi^2\,\Delta\phi_4}{2\,d\,\cos(x_2^0)} \tag{A.28}$$

$$\begin{aligned}\frac{\partial x_3}{\partial \varepsilon} = {} & \big(-2\,\delta\phi\,r\,sin(x_1^0)\,\sin(x_2^0) + \delta\phi^2\,\Delta v_\varepsilon + (6\,d - 7\,R)\,\cos(x_2^0)\,\sin(x_1^0) \\ & +(2\,d - R)\,\cos(x_1^0)\,\sin(x_2^0) + (2\,d - R)\,\sin(x_1^0 + 3\,x_2^0)\big) \\ & \times\frac{1}{2\,d\cos(x_2^0)}\end{aligned} \tag{A.29}$$

The reflection at the disc has to be calculated to get the derivative of θ. The velocity after the bounce $\vec{v}_a$ is given by

$$\vec{v}_a = v\,\vec{n}(x_1'^0 + x_2'^0) - 2\,<v\,\vec{n}(x_1'^0 + x_2'^0) - \vec{v}_s, \vec{x}_e>\vec{x}_e, \tag{A.30}$$

where

$$\vec{v}_s = \vec{n}(x_1^1 + \frac{\pi}{2}) + \varepsilon\,\frac{\partial \vec{g}}{\partial x_1}\,(1 - \varepsilon\,\frac{\partial t}{\partial x_1}\|_{x_1^1}) \tag{A.31}$$

is the velocity of the disc at the reflection.

The velocity vector $\vec{v}_a$ has to be normalized to calculate the derivatives of the cosine of the angle $\theta + \phi + \delta\phi$ and the derivative of the angle θ (A.32. . .A.35).

$$\frac{\partial x_2}{\partial x_2} = \Delta\phi_2 + 2\,\frac{\partial x_3}{\partial x_2} - \frac{2\,R\,\frac{\partial x_3}{\partial x_2}\,\sin(x_2^0)}{v_0} - 1 \tag{A.32}$$

$$\frac{\partial x_2}{\partial x_3} = \Delta\phi_3 + 2\,\frac{\partial x_3}{\partial x_3} - \frac{2\,R\,\frac{\partial x_3}{\partial x_3}\,\sin(x_2^0)}{v_0} \tag{A.33}$$

$$\frac{\partial x_2}{\partial x_4} = \Delta\phi_4 + 2\,\frac{\partial x_3}{\partial x_4} - \frac{2\,R\,\frac{\partial x_3}{\partial x_4}\,\sin(x_2^0)}{v_0} \tag{A.34}$$

$$\begin{aligned}\frac{\partial x_2}{\partial \varepsilon} = {} & \frac{1}{v_0}\left(2\,R\,\sin(x_2^0)\,\sin(x_1^0 + 2\,x_2^0) + v_0\,\frac{\partial x_1}{\partial \varepsilon}\right) \\ & +\frac{1}{v_0}\frac{\partial x_3}{\partial \varepsilon}\,\left(2\,v_0 - 2\,R\sin(x_2^0)\right)\end{aligned} \tag{A.35}$$

Finally one gets the derivative of the Jacobi integral

$$\frac{\partial x_4}{\partial \varepsilon} = \frac{-4\,(d - R)\,R\cos(x_2^0)^2\,\sin(x_1^0 + 2\,x_2^0)}{\delta\phi} \tag{A.36}$$

by using the equations (A.24) and (A.30).

Appendix B

Derivative of $\tilde{f}^m$

The map is given by

$$\begin{pmatrix} \phi_{n+1} \\ \theta_{n+1} \\ \alpha_{n+1} \\ \tilde{J}_{n+1} \\ \varepsilon \end{pmatrix} = \tilde{f} \begin{pmatrix} \phi_n \\ \theta_n \\ \alpha_n \\ \tilde{J}_n \\ \varepsilon \end{pmatrix}. \tag{B.1}$$

Because we restrict us here to a vicinity of periodic orbits the map can be iterated m times. The derivative of $\tilde{f}^m$ of the map (B.1) is nothing else than multiplication by the left for every new bounce with the corresponding 1 bounce derivative.
The abbreviations (B.2)...(B.6) are introduced to simplify the notation.

$$E = \begin{pmatrix} E_{11} = \frac{\partial\theta_{n+1}}{\partial\theta_n} & E_{12} = \frac{\partial\theta_{n+1}}{\partial\alpha_n} \\ E_{21} = \frac{\partial\alpha_{n+1}}{\partial\theta_n} & E_{22} = \frac{\partial\alpha_{n+1}}{\partial\alpha_n} \end{pmatrix} \tag{B.2}$$

$$F = \begin{pmatrix} \frac{\partial\phi_{n+1}}{\partial\theta_n} & \frac{\partial\phi_{n+1}}{\partial\alpha_n} \end{pmatrix} \tag{B.3}$$

$$q = \begin{pmatrix} \frac{\partial\phi_{n+1}}{d\tilde{J}_n} & \frac{\partial\phi_{n+1}}{\partial\epsilon_n} \end{pmatrix} \tag{B.4}$$

$$s = \begin{pmatrix} \frac{\partial\theta_{n+1}}{d\tilde{J}_n} & \frac{\partial\theta_{n+1}}{\partial\epsilon_n} \\ \frac{\partial\alpha_{n+1}}{d\tilde{J}_n} & \frac{\partial\alpha_{n+1}}{\partial\epsilon_n} \end{pmatrix} \tag{B.5}$$

$$t = \begin{pmatrix} \frac{d\tilde{J}_{n+1}}{d\tilde{J}_n} = 1 & \frac{d\tilde{J}_{n+1}}{\partial\epsilon_n} \\ \frac{\partial\epsilon_{n+1}}{d\tilde{J}_n} = 0 & \frac{\partial\epsilon_{n+1}}{\partial\epsilon_n} = 1 \end{pmatrix} \tag{B.6}$$

The derivative of the map (B.1) is then given by

$$D\tilde{f} = \begin{pmatrix} 1 & F & q \\ 0 & E & s \\ 0 & 0 & t \end{pmatrix}. \tag{B.7}$$

In the following the subscript will denote the number of the bounce for the ϕ dependent matrix elements.

The derivative of $\tilde{f}^m$ is given by

$$D\tilde{f}^m = \begin{pmatrix} 1 & F.E(m) & Q(m) \\ 0 & E^m & S(m) \\ 0 & 0 & T(m) \end{pmatrix}, \tag{B.8}$$

where the abbreviations (B.9) ... (B.12) were used.

$$E(m) = \sum_{i=0}^{m-1} E^i \text{ and } E(0) = \begin{pmatrix} 0 & 0 \\ 0 & 0 \end{pmatrix} \tag{B.9}$$

$$T(m) = \prod_{i=1}^{m} t_i \text{ and } T(0) = \mathbb{1} \tag{B.10}$$

$$S(m) = \sum_{i=1}^{m} E^{m-i}\, s_i\, T(i-1) \tag{B.11}$$

$$Q(m) = \sum_{i=1}^{m} \left(q_i\, T(i-1) + F\, E(m-i)\, s_i\, T(i-1)\right) \tag{B.12}$$

proof by induction:

$m = 1$:

$E(1) = \mathbb{1}$
$S(1) = s_1$
$T(1) = t_1$
$Q(1) = q_1$

$$D\tilde{f}^1 = \begin{pmatrix} 1 & F & q_1 \\ 0 & E & s_1 \\ 0 & 0 & t_1 \end{pmatrix} \tag{B.13}$$

$m \to m+1$:

$$D\tilde{f}^{m+1} = \begin{pmatrix} 1 & F & q_{m+1} \\ 0 & E & s_{m+1} \\ 0 & 0 & t_{m+1} \end{pmatrix} \begin{pmatrix} 1 & FE(m) & Q(m) \\ 0 & E^m & S(m) \\ 0 & 0 & T(m) \end{pmatrix}$$

$$
\begin{aligned}
&= \begin{pmatrix} 1 & F\,E(m) + F\,E^m & Q(m) + q_{m+1}\,T(m) + F\,S(m) \\ 0 & E^{m+1} & E\,S(m) + s_{m+1}\,T(m) \\ 0 & 0 & t_{m+1}\,T(m) \end{pmatrix} \\
&= \begin{pmatrix} 1 & F\,(E(m) + E^m) & Q(m) + q_{m+1}\,T(m) + F\,S(m) \\ 0 & E^{m+1} & E\,S(m) + s_{m+1}\,T(m) \\ 0 & 0 & T(m+1) \end{pmatrix}
\end{aligned}
\tag{B.15}
$$

By using the definitions (B.9. . .B.12) the relations (B.16. . .B.18) are fulfilled which completes the proof.

$$
F\,E(m) + F\,E^m = F\,E(m+1) \tag{B.16}
$$

$$
\begin{aligned}
&E\,S(m) + s_{m+1}\,T(m) = E\sum_{i=1}^{m} E^{m-i}\,s_i\,T(i-1) + E^0\,s_{m+1}\,T(m) \\
&= \sum_{i=1}^{m} E^{m+1-i}\,s_i\,T(i-1) + E^{m+1-(m+1)}\,s_{m+1}\,T(m+1-1) \\
&= \sum_{i=1}^{m+1} E^{m+1-i}\,s_i\,T(i-1) = S(m+1)
\end{aligned}
\tag{B.17}
$$

$$
\begin{aligned}
&Q(m) + q_{m+1}\,T(m) + F\,S(m) \\
&= \sum_{i=1}^{m} \left(q_i\,T(i-1) + F\,E(m-i)\,s_i\,T(i-1)\right) + q_{m+1}\,T(m) + F\sum_{i=1}^{m} E^{m-i}\,s_i\,T(i-1) \\
&= \sum_{i=1}^{m+1} q_i\,T(i-1) + F\sum_{i=1}^{m} \left(E(m-i)\,s_i\,T(i-1) + E^{m-i}\,s_i\,T(i-1)\right) \\
&= \sum_{i=1}^{m+1} q_i\,T(i-1) + F\sum_{i=1}^{m} \left((E(m-i) + E^{m-i})\,s_i\,T(i-1)\right) \\
&= \sum_{i=1}^{m+1} q_i\,T(i-1) \\
&+F\sum_{i=1}^{m} \left(E(m+1-i)\,s_i\,T(i-1)\right) + F\,E(m+1-(m+1))\,s_{m+1}\,T(m+1-1) \\
&= \sum_{i=1}^{m+1} q_i\,T(i-1) + F\sum_{i=1}^{m+1} \left(E(m+1-i)\,s_i\,T(i-1)\right) = Q(m+1)
\end{aligned}
\tag{B.18}
$$

Appendix C

Calculation of T(m)

$T(m)$ in (B.10) can easily be calculated and is given by

$$T(m) = \begin{pmatrix} 1 & \sum_{i=1}^{m} \frac{\partial \tilde{J}}{\partial \epsilon}(\phi_i) \\ 0 & 1 \end{pmatrix}. \tag{C.1}$$

Thus the sum should sum up to zero after section 4.2. The angle ϕ_i is the angle at the bounce i and given by $\phi_i = \phi_0 + (i-1)\,\delta\phi$. Basic but helpful relations are given in (C.2) ... (C.5).

$$\sum_{i=0}^{n-1} \cos(\frac{2\pi i k}{n} + a) = 0 \text{ for } k, n \in \mathbb{Z} - \{0\} \tag{C.2}$$

$$\cos(\phi_0)\cos(\phi_1) = \frac{1}{2}(\cos(\phi_0 + \phi_1) + \cos(\phi_0 - \phi_1)) \tag{C.3}$$

$$\sin(\phi_0)\sin(\phi_1) = \frac{1}{2}(\cos(\phi_0 - \phi_1) - \cos(\phi_0 + \phi_1)) \tag{C.4}$$

$$\cos(\phi_0)\sin(\phi_1) = \frac{1}{2}(\sin(\phi_0 + \phi_1) + \sin(\phi_1 - \phi_0)) \tag{C.5}$$

After equation (C.2) all terms which only have cosines and sinus dependence in ϕ_0 will sum up to zero in the matrix element $T(m)$ (C.1). The equations (C.3. . .C.5) shows how multiplication of sinus and cosines terms affect our cosines and sinus terms. We will make some abuse of notations and say that a term is of order k if he has a $\cos(k\,\phi_0 + c)$ dependence, where $k \in \mathbb{Z}$ and $c \in \mathbb{R}$. The above relations show that a term of order k+k' and a term of order k-k' is obtained if a term of order k is multiplied with a term of order k'.

The derivative $\frac{\partial \tilde{J}_{n+1}}{\partial \epsilon}$ must be calculated. Firstly some basic equations for our system will be given, where the subscript 0 means initial conditions and 1 end values. All relations are given to the first order in ϵ. In the following the functions in the first order perturbation are always thought to be in a Fourier series form in the variable ϕ_0 and we denote by $< , >$ the usual scalar product. It has to be mentioned as in Appendix A that the calculation is made in the rest frame.
The Jacobi integral is given by

$$\tilde{J} = \frac{\vec{v}^2}{2} - (x\, v^y - y\, v^x), \tag{C.6}$$

where $\vec{v}$ is the velocity of the projectile, x, y the position and v^x and v^y the velocity of the projectile in the x and y direction. The vector $\vec{n}(\phi) = (\cos(\phi), \sin(\phi))^T$ and the angle difference $\delta\phi = 2\,\theta_0 + (2\,n-1)\pi$ are defined to shorten the equations. The starting position of the projectile is given by

$$\vec{x} = (R-d)\,\vec{n}(\phi_0) + \vec{g}(\phi_0)\,\epsilon, \tag{C.7}$$

where ϵ is the perturbation parameter, d the radius of the disc, ϕ_0 the initial angle of the disc and $g(\phi)$ indicates perturbed movement of the disc. The velocity of the periodic orbits for the circular case is $v_0 = \frac{-2\,\cos(\theta_0)}{\delta\phi}(R-d)$ (see section 4.3.2). The starting velocity is given by

$$\vec{v_0} = (v_0 + \epsilon\, dv)\,\vec{n}(\theta_0 + \phi_0), \tag{C.8}$$

where dv is the velocity change under perturbation, so that the Jacobi integral (C.6) is constant. Because the Jacobi integral (C.6) and the angles θ_0 and ϕ_0 has to be constant dv is given by

$$dv = \frac{\vec{g}(\phi_0)^x\, \sin(\phi_0+\theta_0) - \vec{g}(\phi_0)^y\, \cos(\phi_0+\theta_0)}{v_0 - (R-d)\, \sin(\theta_0)} v_0, \tag{C.9}$$

where $\vec{g}(\phi_0)^x$ resp. $\vec{g}(\phi_0)^y$ is the x resp. y component of the perturbation. The time has the ϕ dependence indicated in equation (C.10).

$$t(\phi) = \phi + \epsilon h(\phi) \tag{C.10}$$

The reflecting position of the particle is given by the equation (C.13). The change of the angle ϕ, where the projectile hits the disc, due to the perturbation is denoted by $d\phi_0$. Additionally the abbreviations (C.11) and (C.12) are introduced.

$$\phi_1 \;=\; \phi_0 + \delta\phi \tag{C.11}$$

$$\begin{aligned}
\phi_1' &= \phi_1 + \varepsilon\, d\phi_0 && \text{(C.12)}\\
\vec{x}_1 &= \vec{x} + (v_0\,(t(\phi_1') - t(\phi_0)) + dv\,\epsilon\,\delta\phi)\,\vec{n}(\phi_0 + \theta_0)\\
&= \vec{x} + v_0\,\delta\phi\,\vec{n}(\phi_0 + \theta_0)\\
&+ \epsilon\,(v_0\,h(\phi_1) - v_0\,h(\phi_0) + v_0\,d\phi_0 + dv\,\delta\phi)\,\vec{n}(\phi_0 + \theta_0) && \text{(C.13)}
\end{aligned}$$

The abbreviation (C.15) leads to the equation (C.14).

$$\begin{aligned}
\vec{x}_1 &= \vec{x} + \epsilon\, dx_1\,\vec{n}(\phi_0 + \theta_0) + v_0\,\delta\phi\,\vec{n}(\phi_0 + \theta_0) && \text{(C.14)}\\
dx_1 &= v_0\,h(\phi_1) - v_0\,h(\phi_0) + v_0\,d\phi_0 + dv\,\delta\phi && \text{(C.15)}
\end{aligned}$$

The normal vector of the surface at the reflection point is then given by

$$\vec{n}_n = \frac{1}{d}(\vec{x}_1 - R\,\vec{n}(\phi_1) - \epsilon\,(\vec{g}(\phi_1) + R\,d\phi_0\,\vec{n}(\phi_1 + \pi/2))). \tag{C.16}$$

The velocity after the reflection is

$$\vec{v}_1 = \vec{v}_0 - 2\ <\vec{v}_0 - \vec{v}_s, \vec{n}_n>\vec{n}_n, \tag{C.17}$$

where $\vec{v}_s$ is the velocity of the disc.

The derivative of the angle ϕ with respect to the time has to be known to calculate the velocity of the disc $\vec{v}_s$. The change of this derivative due to the function $h(\phi)$ in the formula (C.10) is given by

$$\frac{d\phi}{dt} = 1 - \epsilon\frac{\partial h}{\partial \phi}\ |_{\phi=t}, \tag{C.18}$$

where the angle ϕ is substituted by the time t.

This result leads to the velocity of the disc

$$\vec{v}_s = R\,\vec{n}(\phi_1 + \pi/2) + \epsilon\,(-R\,d\phi_0\,\vec{n}(\phi_1) + \frac{\partial \vec{g}(\phi)}{\partial \phi}(\phi_1) - R\,\frac{\partial h}{\partial \phi}\ |_{\phi_1}\ \vec{n}(\phi_1 + \pi/2)). \tag{C.19}$$

The equation

$$(\vec{x}_1 - R\,\vec{n}(\phi_1) - \epsilon\,(\vec{g}(\phi_1) + R\,d\phi_0\,\vec{n}(\phi_1 + \pi/2)))^2 = d^2 \tag{C.20}$$

must be fulfilled at the moment when the projectile hits the disc.
Due to the expression (C.20) the angle difference

$$d\phi_0 = -\frac{<\vec{n}(\phi_1), \vec{g}(\phi_0) - \vec{g}(\phi_1)>}{\cos(\theta_0 - \delta\phi)\,v_0} - (h(\phi_1) - h(\phi_0)) - \frac{dv\,\delta\phi}{v_0} \tag{C.21}$$

is calculated. For the derivation of the sum in the matrix (C.1) it is important to notice that in $d\phi_0$ (C.21) one divides by terms which are independent of ϕ_0.

The different addend of the derivative of the equation (C.17) at $\epsilon = 0$ are shown below(C.22...C.27).

$$
\begin{aligned}
I &= \frac{\partial \vec{v}_0}{\partial \epsilon} = dv\, \vec{n}(\phi_0 + \theta_0) && \text{(C.22)}\\
II &= < \frac{\partial \vec{v}_0}{\partial \epsilon}, \vec{n}_n > = -dv \cos(\theta_0 - \delta\phi) && \text{(C.23)}\\
III &= < \vec{v}_0, \frac{\partial \vec{n}_n}{\partial \epsilon} > = \frac{v_0}{d} \left(dx_1 + < \vec{n}(\phi_0 + \theta_0), \vec{g}(\phi_0) - \vec{g}(\phi_1) > \right)\\
&- \frac{v_0\, R\, d\phi_0}{d} \cos(\theta_0 - \delta\phi - \pi/2) && \text{(C.24)}\\
IV &= < \frac{\partial \vec{v}_s}{\partial \epsilon}, \vec{n}_n > = R\, d\phi_0 + < \frac{\partial \vec{g}}{\partial \phi}(\phi_1), \vec{n}(\phi_1 + \pi) > && \text{(C.25)}\\
V &= < \vec{v}_s, \frac{\partial \vec{n}_n}{\partial \epsilon} > = \frac{R}{d} \left(-R\, d\phi_0 + dx_1\, \sin(\theta_0 - \delta\phi) \right)\\
&+ \frac{R}{d} \left(< \vec{n}(\phi_1 + \pi/2), \vec{g}(\phi_0) - \vec{g}(\phi_1) > \right) && \text{(C.26)}\\
VI &= \cos(\theta_0 - \delta\phi)\, \frac{1}{d} (\vec{g}(\phi_1) - \vec{g}(\phi_0) + R\, d\phi_0\, \vec{n}(\phi_1 + \pi/2))\\
&- dx_1\, \vec{n}(\phi_0 + \theta_0)\, \cos(\theta_0 - \delta\phi)\, \frac{1}{d} && \text{(C.27)}
\end{aligned}
$$

The derivative of the velocity is then given by

$$\frac{\partial v_1}{\partial \epsilon} = I - 2(II + III - IV - V)\, \vec{n}(\phi_1 + \pi) - 2\, VI. \qquad \text{(C.28)}$$

The derivative of $\tilde{J}$ (C.6) after the bounce at ϕ_1 for $\epsilon = 0$ can be calculated by

$$\frac{\partial \tilde{J}}{\partial \epsilon} = < \vec{v}_1, \frac{\partial \vec{v}_1}{\partial \epsilon} > - \left(\frac{\partial \vec{v}_1^{\,y}}{\partial \epsilon}\, \vec{x}_1^{\,x} + \frac{\partial \vec{x}_1^{\,x}}{\partial \epsilon}\, \vec{v}_1^{\,y} - \frac{\partial \vec{v}_1^{\,x}}{\partial \epsilon}\, \vec{x}_1^{\,y} - \frac{\partial \vec{x}_1^{\,y}}{\partial \epsilon}\, \vec{v}_1^{\,x} \right). \qquad \text{(C.29)}$$

The order of the terms without derivative in equation (C.29) are trivially one, because of the results (C.30) and (C.31).

$$
\begin{aligned}
\vec{v}_1(\epsilon = 0) &= v_0\, \vec{n}(\phi_0 + \delta\phi + \theta_0) && \text{(C.30)}\\
\vec{x}_1(\epsilon = 0) &= (R - d)\, \vec{n}(\phi_0 + \delta\phi) && \text{(C.31)}
\end{aligned}
$$

All multiplications of the derivative of $\tilde{J}$ (C.29) are by a factor of order 1. Thus, if there are no first–order terms in all derivatives, the sum will add up to zero.

The derivative of $\vec{x}_1$ is given by

$$\frac{\partial \vec{x}_1}{\partial \epsilon} = \vec{g}(\phi_0) + \vec{n}(\phi_0)\, dx_1. \qquad \text{(C.32)}$$

This derivative has no first–order terms, if $\vec{g}(\phi_0)$ has no first–order terms and dx_1 has no zeroth– and second–order terms.

The above relations (C.28) for the derivative of v_1 yield that if equation I (C.22) and VI (C.27) have no first–order term and equations II (C.23) to V (C.26) have no zeroth– and second–order term, then the sum in the matrix (C.1) will sum up to zero.

The equation I has no first–order term if dv has no zeroth– and second–order terms. The equation VI (C.27) has no first–order term if g has no first–order and $d\phi_0$ resp. dx_1 has no zeroth– and second–order terms.
From the derivatives II (C.23) to V (C.26) the new conditions that g should not have terms of order -1 and 3 are obtained.

The condition (C.21) on $d\phi_0$ imposes only one new condition, namely that h has no zeroth and second–order terms. The conditions on dx_1(C.15) and dv (C.9) do not contribute further conditions on h and g.

The sum will surely be zero if h contains no zeroth and second–order terms and if g contains no terms of order -1, 1, and 3.

It should be mentioned that the above conditions on g and h are sufficient but not necessary conditions on these perturbation functions.

Appendix D

Calculation of $\det$(B(m))

The determinant of the matrix $\mathbf{B}(m)$ (4.14) can be calculated with the derivatives in Appendix A and the derivative in Appendix B. Because the matrix $\mathbf{B}(m)$ is independent of the perturbation the determinant is it, too. The same abbreviations as in the Appendix B are taken, except the first component of q resp. the first column of s will be denoted by r_0 resp. $u = (u_x, u_y)^T$. Thus the matrix Df is given by

$$Df = \begin{pmatrix} 1 & F & r_0 \\ 0 & E & u \\ 0 & 0 & 1 \end{pmatrix}. \tag{D.1}$$

Using this abbreviations the matrix

$$\mathbf{B}(m) = \begin{pmatrix} F\,E(m) & r(m) \\ E^m - \mathbb{1} & u(m) \end{pmatrix} \tag{D.2}$$

is obtained. The results in Appendix B, $r(m)$ and $u(m)$ leads to the expressions (D.3) and (D.4).

$$r(m) = m\,r_0 + F \sum_{i=1}^{m} E(m-i) \begin{pmatrix} u_x \\ u_y \end{pmatrix} \tag{D.3}$$

$$u(m) = E(m) \begin{pmatrix} u_x \\ u_y \end{pmatrix} \tag{D.4}$$

If the eigenvalues $(\lambda, 1/\lambda)$ of the matrix E are not ± 1 then the matrix can be diagonalized as written in equation (D.5).

$$E = a \begin{pmatrix} \lambda & 0 \\ 0 & 1/\lambda \end{pmatrix} a^{-1} \tag{D.5}$$

The results for E^m, $E(m)$ and the second part in $r(m)$ (D.4) are given in the equations (D.6. . .D.8).

$$E^m = a \begin{pmatrix} \lambda^m & 0 \\ 0 & \frac{1}{\lambda^m} \end{pmatrix} a^{-1} \tag{D.6}$$

$$\begin{aligned} E(m) &= \sum_{i=0}^{m-1} E^i = a(\sum_{i=0}^{m-1} \begin{pmatrix} \lambda^i & 0 \\ 0 & \frac{1}{\lambda^i} \end{pmatrix}) a^{-1} \\ &= a \begin{pmatrix} \frac{1-\lambda^m}{1-\lambda} & 0 \\ 0 & \frac{1-1/\lambda^m}{1-1/\lambda} \end{pmatrix} a^{-1} \end{aligned} \tag{D.7}$$

$$\begin{aligned} \sum_{i=1}^{m} E(m-i) &= a \sum_{i=0}^{m-1} \begin{pmatrix} \frac{1-\lambda^i}{1-\lambda} & 0 \\ 0 & \frac{1-1/\lambda^i}{1-1/\lambda} \end{pmatrix} a^{-1} \\ &= a \begin{pmatrix} \frac{m-m\,\lambda-1+\lambda^m}{(1-\lambda)^2} & 0 \\ 0 & \frac{m-m\,/\lambda-1+\lambda^{-m}}{(1-1/\lambda)^2} \end{pmatrix} a^{-1} \end{aligned} \tag{D.8}$$

The determinant of $\mathbf{B}(m)$ is then given by

$$\det(\mathbf{B}(m)) = \frac{m(\lambda^m - 1)^2}{\lambda^m\,(\lambda - 1)}\,C. \tag{D.9}$$

The variable C is independent of m. Thus if this determinant is not 0 for one bounce then it can only be zero if $\lambda^m = 1$. The determinant for one bounce can be calculated using the Appendix A and is given by

$$\det(\mathbf{B}(1)) = -\frac{R\,\delta\phi^3}{d\,(R-d)^2\,\cos(\theta_0)^2}. \tag{D.10}$$

Appendix E

Bifurcation for small Jacobi integral

If the disc moves on a circular orbit the trace of the derivative of the symplectic map is given by

$$TrD\mathcal{P}_{\tilde{J}} = \frac{2\,\tilde{d} + (\delta\phi^2 - 4) - 4\,\delta\phi\,\tan(\theta) - \delta\phi^2\,\tan(\theta)^2}{\tilde{d}}. \tag{E.1}$$

For large n the trace (E.1) is approximately 2 at $\tilde{\theta}_n^-(0)$ (E.2) and approximately -2 at $\tilde{\theta}_n^-(\tilde{d})$ for negative Jacobi integral.

$$\tilde{\theta}_n^-(\tilde{d}) = \frac{3\,\pi}{4} - \frac{\left(4\,\left(\tilde{d} - 1\right) + 2\,\pi + 8\,n\,\pi\right)}{(4 - 16\,n\,\pi + \pi^2\,(1 + 4\,n)^2)} \tag{E.2}$$

For positive Jacobi integral and large n the trace (E.1) is approximately 2 for an angle of $\tilde{\theta}_n^+(0)$ (E.3) and approximately -2 for $\tilde{\theta}_n^+(\tilde{d})$.

$$\tilde{\theta}_n^+(\tilde{d}) = \frac{5\,\pi}{4} - \frac{\left(4\,(1 - \tilde{d}) + 6\,\pi + 8\,n\,\pi\right)}{(8 + 12\,\pi + 16\,n\,\pi + \pi^2\,(3 + 4\,n)^2)} \tag{E.3}$$

The value of the Jacobi integral for $TrD\mathcal{P}_{\tilde{J}} = 2$ in first order of $1/n$ is $\pm\frac{1}{2\,\pi\,n}$, where the signs corresponds to the positive resp. negative Jacobi integral. The difference between the Jacobi integral for the trace equals 2 and the trace equals -2 in orders of $1/n$ is given by $\tilde{J}_{Tr=2} - \tilde{J}_{Tr=-2} = \mathrm{sgn}(\tilde{J})\frac{\tilde{d}\,(4+\tilde{d})}{16\,\pi^5\,n^5}$.

This indicates that the elliptic fixed point gets always inverse hyperbolic before the next bifurcation occurs. Because the derivative in Figure 4.3 is high we think that

the whole system gets completely hyperbolic before the next two fixed points were born.

Appendix F

Poincaré maps

In the following, we show the symplectic Poincaré maps (4.24) for the case when the disc is moving on a circular orbit. Only the stable and the unstable manifold of the interesting part are plotted. The other part of the unstable resp. stable manifold, which is connected to the fixed point, just goes straight away. In all figures the unstable manifold is plotted in black, the stable manifold in red and the boundary of the domain in blue. In a few graphs the fixed points which were created through a saddle–center bifurcation are shown as magenta crosses and some orbits are shown in green. The maxima of the scaled Jacobi integral J_n (4.28) are located approximately at $J_0 \approx 0.2933$ and $J_1 \approx 0.10107$ and the minima are at approximately $J_1 \approx -0.11443$ and $J_2 \approx -0.06635$. For an explanation of the Poincaré maps and the bifurcation scenario shown in the following figures, see also section 4.3.3.

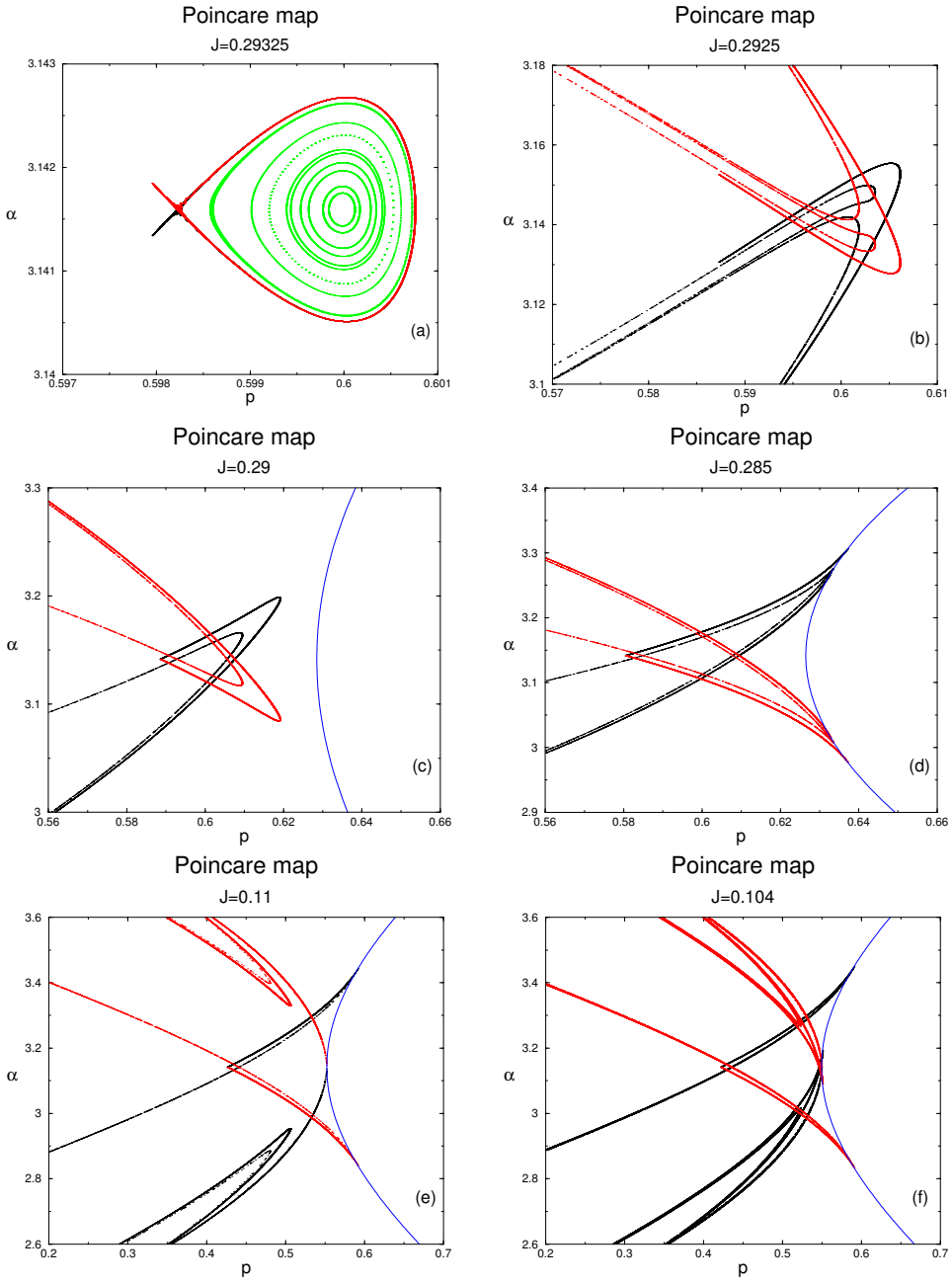

Figure F.1: (a) The value of the Jacobi integral is just after the first saddle–center bifurcation J_0^{max}. (b) This figure corresponds almost to the case shown in Figure 4.4 (a). (c) A complete binary horseshoe is seen (see also Figure 4.4 (b)). (d) The stable and unstable manifold touch the boundary of the definition domain. (e) The stable manifold resp. unstable manifold is folded back to the fundamental rectangle, but has no homoclinic intersection with the fundamental rectangle. (f) This figure corresponds to the schematic case shown in Figure 4.4 (c).

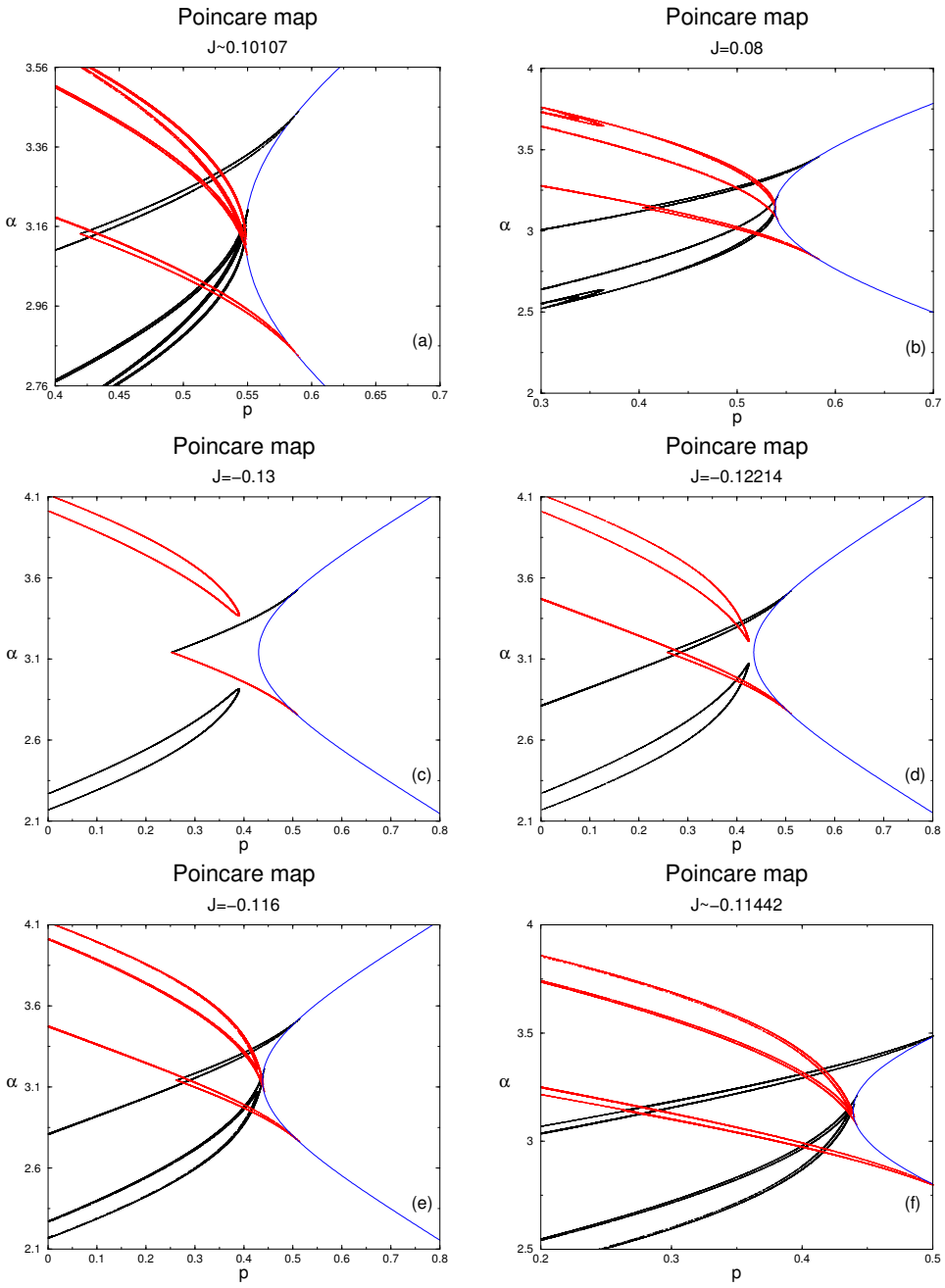

Figure F.2: (a) This figure shows the case of the second saddle–center bifurcation $J \approx J_1^{max}$. (b) The complete quartenary horseshoe is reached as in the schematic Figure 4.4 (d). In the following the Jacobi integral is negative. (c) One fixed points exist, but there are no homoclinic intersections. (d) In this figure first homoclinic intersections occurred. (e) The tendrils intersects each other and the dynamics can be described by an incomplete ternary horseshoe (see Figure 4.6 (a)). (f) The case of the first saddle–center bifurcation for negative Jacobi integral $J \approx J_1^{min}$ is shown.

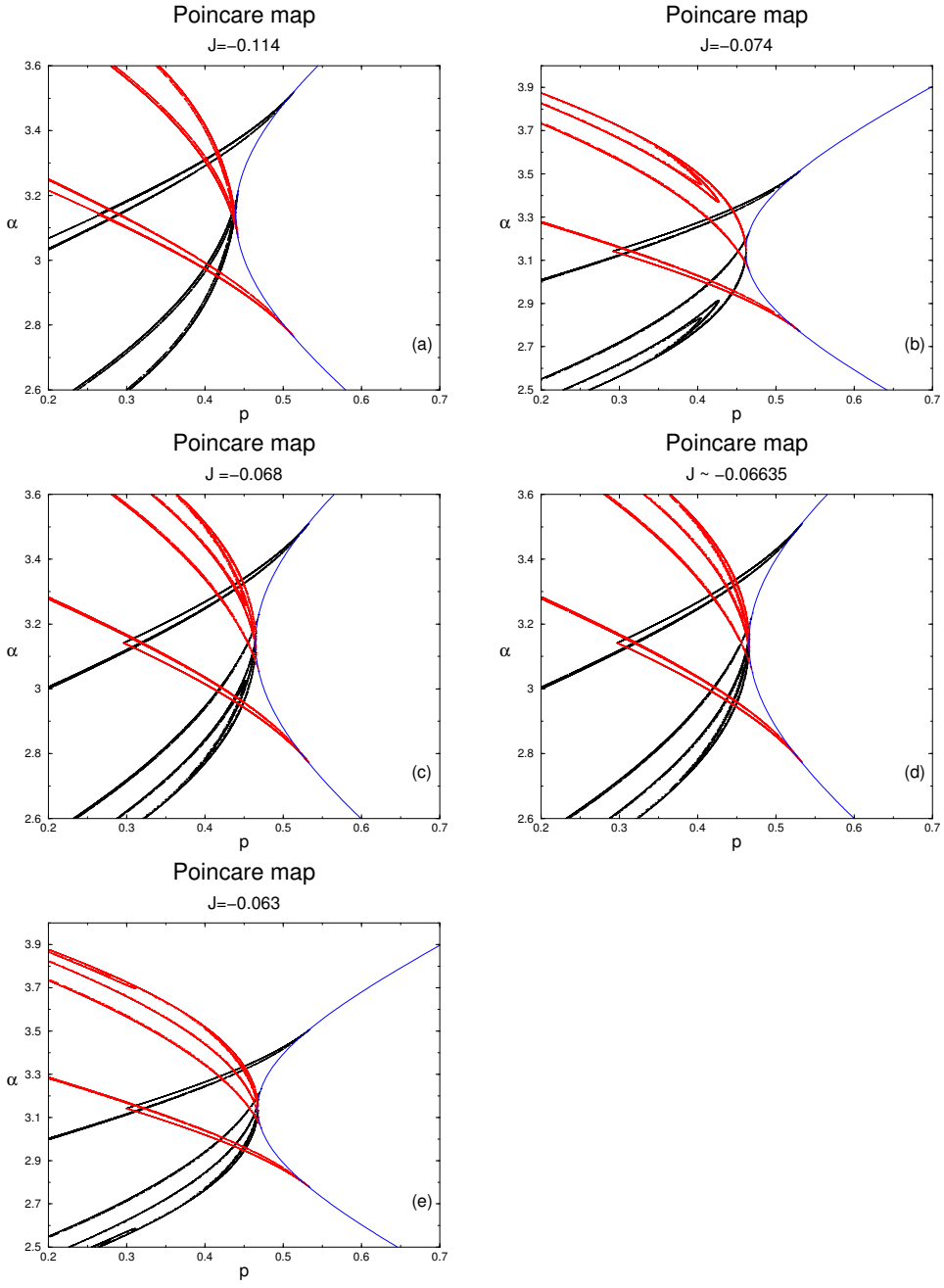

Figure F.3: (a) A complete ternary horseshoe dynamics is reached (see Figure 4.6 (b)) and (b) the folding back of the tendrils is seen. (c) The tendrils had some homoclinic intersections (corresponds to Figure 4.6 (c)). (d) This Figure shows the case of the second saddle–center bifurcation for negative Jacobi integral $J \approx J_2^{min}$. (e) The complete quintuple horseshoe is reached (see also Figure 4.6 (d)).

Appendix G

Derivative of the 4D symplectic map for the circular case

The derivative of the periodic orbits of the 4D–symplectic map of the article of Dullin [31] can be calculated for the disc moving on a circular orbit. The first coordinate is the arc–length with the canonical conjugate variable p (4.23). The other two coordinates are given by the time resp. the angle ϕ and the Jacobi integral J. In the derivative (G.1) the radius R was set to 1 to shorten the equation.

$$\begin{pmatrix} \frac{(d-2+(d-2+\delta\phi)\,\cos(2\,\theta)-2\,\delta\phi\sin(2\,\theta))}{2\,d\cos^2(\theta)} & 0 & \frac{\delta\phi\left((\delta\phi^2-2)\cos(2\,\theta)-2-2\,\delta\phi\,\sin(2\,\theta)\right)}{4\,\cos^4(\theta)} & \frac{\delta\phi^2(\delta\phi\,\cos(2\,\theta)-\sin(2\,\theta))}{4\,(d-1)\,\cos^4(\theta)} \\ \frac{\delta\phi\left(\delta\phi-2\,\tan(\theta)-\delta\phi\,\tan^2(\theta)\right)}{2\,(d-1)\,d} & 1 & \frac{\delta\phi^2(\delta\phi\cos(2\,\theta)-\sin(2\,\theta))}{4\,(d-1)\,\cos^4(\theta)} & \frac{\delta\phi^3\,\cos(2\,theta)}{4\,(1-d)^2\,\cos^4(\theta)} \\ \frac{\left(2d-2+(\delta\phi^2+2d-2)\cos(2\,\theta)-2\delta\phi\,\sin(2\,\theta)\right)}{d^2\,\delta\phi} & 0 & \frac{\left(d-2+(\delta\phi^2+d-2)\,\cos(2\,\theta)-2\,\delta\phi\,\sin(2\,\theta)\right)}{2\,d\cos^2(\theta)} & \frac{\delta\phi\left(\delta\phi-2\,\tan(\theta)-\delta\phi\,\tan^2(\theta)\right)}{2\,(d-1)\,d} \\ 0 & 0 & 0 & 1 \end{pmatrix} \tag{G.1}$$

The matrix (G.1) has two eigenvalues of 1. One eigenvector to an eigenvalue 1 is given by $(0,1,0,0)^T$. The Krein signature (2.9) corresponding to this eigenvector is 0, so the Krein signature is not of definite sign and thus bifurcations as described in section 2.6 can occur.

Appendix H

Two–bounce periodic orbits

The periodic orbits for 2 bounces of the map f_0 (H.1) are given by $\alpha = \theta = \pi$, $\tilde{J} = \frac{2\,(1-\tilde{d})^2\,R^2}{\pi^2}$ and ϕ arbitrary.

$$\begin{pmatrix} \phi_{n+1} \\ \alpha_{n+1} \\ \theta_{n+1} \\ \tilde{J}_{n+1} \end{pmatrix} = f_\varepsilon \begin{pmatrix} \phi_n \\ \alpha_n \\ \theta_n \\ \tilde{J}_n \end{pmatrix}. \tag{H.1}$$

The linear equations (4.14) can be calculated using the derivatives in Appendix B and A. The eccentricity ε and angle ϕ–dependence of the periodic orbits of the map (H.1) is given in equation (H.2).

$$\begin{pmatrix} \phi \\ \theta \\ \alpha \\ \tilde{J} \end{pmatrix} = \begin{pmatrix} \phi_0 \\ \pi \\ \pi \\ \frac{2\,(1-\tilde{d})^2\,R^2}{\pi^2} \end{pmatrix} - \varepsilon \begin{pmatrix} 0 \\ (\pi^2 + 8\,\tilde{d} - 8) \\ (\pi^2 + 8\,\tilde{d} - 8) \\ \frac{2\,(\tilde{d}-1)\,R^2\,(\pi^2+4\,\tilde{d}-4)}{\pi} \end{pmatrix} \frac{\sin(\phi_0)}{(\pi^2 + 4\,\tilde{d} - 4)} \tag{H.2}$$

Bibliography

[1] Jung C and Scholz H J. Chaotic scattering off the magnetic dipole. *Journal of Physics A*, 21:2301–2310, 1988.

[2] Eckhardt B. Fractal properties of scattering singularities. *Journal of Physics A*, 20:5971–5980, 1987.

[3] Jackson E A. *Perspectives of Nonlinear Dynamics*. Cambridge University Press, Cambridge, 1991.

[4] Wiggins S. *Chaotic Transport in Dynamical Systems*. Springer, New York Berlin, 1992.

[5] Jaffe C et al. the geometry of reaction dynamics. *Nonlinearity*, 15:947–992, 2002.

[6] Jung C Bütikhofer T and Seligman T H. Extraction of information about periodic orbits from scattering functions. *Physics Letters A*, 265:76–82, 2000.

[7] Mejia-Monasterio C Jung C and Seligman T H. Quantum and classical echoes in scatttering systems described by simple smale horseshoes. *Europphysics Letters*, 55:616–622, 2001.

[8] Lipp C Jung C and Seligman T H. The inverse scattering problem for chaotic hamiltonian systems. *Annals of Physics*, 275:151–189, 1999.

[9] Merlo O Jung C and Seligman T H. Symmetry properties of periodic orbits extracted from scattering data. *Chaos*, 14:969–974, 2004.

[10] Szebehely V G. *Theory of Orbits: The Restricted Problem of Three Bodies*. Academic Press, New York, 1967.

[11] Arnold V I. *Mathematical Methods of Classical Mechanics*. Springer, New York Berlin, 1989.

[12] Krein M G. *Topics in differential and integral equations and operator theory*. Birkhäuser Verlag, Basel, 1983.

[13] Skokos Ch. on the stability of periodic orbits of high dimensional autonomous hamiltonian systems. *Physica D*, 159:155–179, 2001.

[14] Howard J E and Dullin H R. Linear stability of natural symplectic maps. *Physica D*, 246:273–283, 1998.

[15] Grebogi C. Output functions and fractal dimensions in dynamical systems. *Pysics Review Letters*, 86:2778–2781, 2001.

[16] Ott E and Tel T. chaotic scattering: an introduction. *Chaos*, 3:417–426, 1993.

[17] Perko L. *Differential Equations and Dynamical Systems*. Springer, New York Berlin, 1991.

[18] Wiggins S. *Introduction to Applied Nonlinear Dynamical Systems and Chaos*. Springer, New York Berlin, 2003.

[19] Jung C and Rückerl B. Scaling properties of a scattering system with an incomplete horseshoe. *Journal of Physics A*, 27:55–77, 1994.

[20] Wiggins S. *Introduction to Applied Nonlinear Dynamical Systems and Chaos*. Springer, New York Berlin, 1990.

[21] Jaffé C et al. impenetrable barriers in phase-space. *Physical Review Letters*, 86:6478–5481, 2001.

[22] Wiggins S. *Global Bifurcations and Chaos*. Springer, New York Berlin, 1988.

[23] Beck C and Schlögl F. *thermodynamics of chaotic systems, an introduction*. Cambridge University Press, Cambridge, 1993.

[24] Bohr T and Rand D. The entropy function for characteristic exponents. *Physica D*, 25:387–398, 1987.

[25] Bountis T Ding M and Ott E. Algebraic escape in higher dimensional hamiltonian system. *Physics Letters A*, 151:395–400, 1990.

[26] Karney C. Long time correletions in the stochastic regime. *Physica D*, 8:360–380, 1983.

[27] Pikovsky A S. Escape rate for transient chaos and chaotic scattering in non-hyperbolic hamiltonian systems. *Journal of Physics A*, 25:L477–L481, 1992.

[28] Grebogi C Lai Y-C, Ding M and Blümel R. algebraic decay and fluctuations of the decay exponent in hamiltonian systems. *Physical Review A*, 46:4661–4669, 1992.

[29] Chirikov B V and Shepylansky D L. Asymptotic statistics of poincaré recurrences in hamiltonian systems with divided phase space. *Physical Review Letters*, 82:528–531, 1999.

[30] Benet L et al. chaotic scattering of a rotating target. *Journal of Physics A*, 28:2529–2544, 1995.

[31] Dullin H R. Linear stability in billiards with potential. *Nonlinearity*, 11:151–173, 1998.

[32] Moser J K and Siegel C L. *Lectures on Celestial Mechanics*, chapter the continuation method. Springer-Verlag, Berlin Heidelberg, 1971.

[33] Whittaker E T. *a treatise on the analytical dynamics of particles and rigid bodies*. Cambridge University Press, Cambridge, 1989.

[34] Howard J E and MacKay R S. Linear stability of symplectic maps. *J Math Phys*, 28:1036–1051, 1987.

[35] Kuznetsov Y A. *Elements of Applied Bifurcation Theory*. Springer, New York Berlin, 1995.

[36] Goldstein H. *classical mechanics*. Addison Wesley, San Francisco, 2002.

[37] Seligman T H Benet L. generic occurence of rings. *Physics Letters A*, 273:331–337, 2000.

[38] Seligman T H Benet L. occurence of planetary rings with shepherds. *Celestial mechanics and Dynamical Astronomy*, 81:123–128, 2001.

[39] Klebanoff A Davidchak R L, Lai Y and Bollt M. towards complete detection of unstable periodic orbits in chaotic systems. *Physics letters A*, 287:99–104, 2001.

Dank

Es sind $3\frac{1}{2}$ Jahre seit Begin der Dissertation vergangen. Viele Menschen sind mir während dieser Zeit zur Seite gestanden.
An erster Stelle möchte ich dem Doktorvater T.H. Seligman aus dem fernen Mexico danken, der zwar selten physisch in Basel war, aber doch immer ein offenes Ohr für meine mehr oder weniger verrückten Ideen hatte. Die Aufenthalte in Mexico, wo ich seine Gastfreundschaft habe erleben dürfen, werden mir immer in Erinnerung bleiben.
Zusätzlich möchte ich meinem anderen Doktorvater D. Trautmann für die herzliche Aufnahme in sein Team und die mir ermöglichte freie Arbeitsweise danken. Ich hoffe, dass ich ihm mit dieser Doktorarbeit etwas zurückgeben kann.
Luis Benet und Christoph Jung danke ich für ihre hervorragende Unterstützung in technischen Fragen. Sie haben mir, jeder auf seine Art, sehr bei dieser Doktorarbeit geholfen.
Mein Dank gilt auch den Gruppenmitgliedern Andreas, Florian, Kai, Marc und Ute für die angeregten Diskussionen bei Kaffee und beim Eurograd.
Meinem Büromitbewohner Oliver Gywath danke ich für seine Geduld, mir beim Denken zu zuhören, und für die Durchsicht meiner Dissertation. Zudem brachte er ein bisschen Abwechslung in den normalerweise ernsten Büroalltag.
Nun möchte ich noch meiner ganzen Familie und meiner Freundin Sabine danken, die mich immer und in jeder Beziehung unterstützt und motiviert haben.
Zum Schluss danke ich Calvin und Hobbes für die zahlreichen Aufheiterungen.

Curriculum Vitae

5. Mai 1969	geboren in Liestal
1976-1981	Besuch der Primarschule in Waldenburg BL (erstes Schuljahr) und Hölstein BL
1981-1985	Besuch der Sekundarschule (erstes Jahr) und des Progymnasiums in Oberdorf BL
1985-1988	Lehre als Chemielaborant bei der Firma Bachem AG in Bubendorf BL
1989-1992	Besuch der Fachhochschule beider Basel in Muttenz BL
1992-1994	Chemiker bei der Firma Siegfried AG in Zofingen AG
1995	Chemiker bei der Firma Rohner AG in Pratteln BL
1995-1999	Studium der Physik an der Universität Fribourg FR
1996	Physikpraktikum bei der ABB in Dättwil AG
1997	Physikpraktikum am PSI in Villigen AG
1998	Physikpraktikum am BNL auf Long Island USA
1999	Diplomarbeit über *Untersuchung der Brechung der Symmetrie des 3 Scheibenbilliards* unter der Anleitung von Prof. Dr. D. Trautmann, Prof. Dr. D. Baeriswyl und Prof. Dr. T. H. Seligman
2000-2004	Doktorarbeit über *Through symmetry breaking to higher dimensional chaotic scattering* an der Universität von Basel unter der Anleitung von Prof. Dr. L. Benet, Prof. Dr. C. Jung Prof. Dr. T. H. Seligman und Prof. Dr. D. Trautmann,

Meine Ausbildung an der Universität Basel und Fribourg und der EPFL verdanke ich den folgenden Dozentinnen und Dozenten.

Dr. P. Aebi, Prof. Dr. A. Antille, Dr. P. Bader, Prof. Dr. D. Baeriswyl, Prof. Dr. X. Bagnoud, Prof Dr. J. P. Berrut, Prof. Dr. J. C. Dousse, Prof. Dr. S. Drissi, Prof. Dr. J. P. Gabriel, Dr. T. Heim. Dr. K. Hencken, Prof. Dr. H. Holmann, Prof. Dr. Ingold, Prof. Dr. B. Kaupp, Prof. Dr. R. Kellerhals, Prof. Dr. J. Kern, Prof. Dr. H. Kleisli, Dr. R. Kunz, Prof. Dr. P. Martin, Dr. F. Meylan, Dr. C. de Morais Smith, Dr. F. Muhlhauser, Dr. R. M. Noack, Prof. Dr. D. Pavuna, Dr. G. Ribordy, Dr. P. de los Rios, Prof. Dr. E. Ruh, Prof. Dr. H. K. Rummler, Prof. Dr. L. Schaller, Prof Dr. L. Schellenberg, Prof. Dr. L. Schlapbach, Prof. Dr. H. Schneuwly, Prof. Dr.

R. Strebel, Prof. Dr. Y. C. Zhang, Prof. Dr. X. Zhotos.